ENERGY PRODUCTION, TRANSPORTATION AND ENVIRONMENTAL EFFECTS

EDITOR
Serkan GÜLDAL

AUTHORS
Ayşe ÇOBAN
Erdal ÇILĞIN
Fatih ISSI
İbrahim YUKSEL
Orhan ÇOBAN

İKSAD
Publishing House

ENERGY PRODUCTION, TRANSPORTATION AND ENVIRONMENTAL EFFECTS

EDITOR

Serkan GÜLDAL

AUTHORS

Ayşe ÇOBAN

Erdal ÇILĞIN

Fatih ISSI

İbrahim YUKSEL

Orhan ÇOBAN

İKSAD Publishing House

(The Licence Number of Publicator: 2014/31220)
TURKEY TR: +90 342 606 06 75
USA: +1 631 685 0 853
E mail: iksadyayinevi@gmail.com
www.iksadyayinevi.com

ISBN: 978-625-8061-10-9
Cover Design: İbrahim KAYA
December / 2021
Ankara / Turkey
Size = 16x24 cm

CONTENTS

PREFACE

The importance of energy is an indisputable truth. Thus, cheaper energy is a hot field of research. The research starts to produce a cheap and efficient way to generate renewable energy. The research continues with its transportation where it is needed. The researchers also consider environmental effects.

This book covers all these questions in six chapters. In the first two chapters, one of the well known renewable energy source, namely Biofuel, is introduced by example studies. The chapters are titled "*Experimental Investigation of Salvia Candidissima Plant in Search of New and Renewable Biofuel*" and "*Investigation of Menntha Tomentosa Oil in Seeking a Biofuel Resource*". After energy generation is explained, some methods are proposed or energy transportation in chapter three "Class-E Resonant Power Converter Design for Wireless Power Transmission Systems" and four "*Magnetic Resonance Coupled Wireless Power Transmission Systems for Electric Vehicles*". In the next chapter, the importance of nuclear energy is discussed in "*The Increasing Importance of Energy and Nuclear Energy*". Lastly, in chapter 6, the environmental effects of hydropower plants in Turkey are explained in "*An Investigation the Effects of the Hydropower Plants on Climate Change and Environmental Issues in Turkey*". For the chapters, all responsibilities belong to the authors.

We are appreciated of authors for their contribution and IKSAD publishing house. We hope this book informs the reader about recent researches about energy.

Assist. Prof. Serkan GÜLDAL

December, 2021

CHAPTER 1

EXPERIMENTAL INVESTIGATION OF SALVIA CANDIDISSIMA PLANT IN SEARCH OF NEW AND RENEWABLE BIOFUEL

Assoc. Prof. Dr. Erdal ÇILĞIN[1]

[1] Dicle University Technical Sciences Angel School, Department of Motor Vehicles and Transportation Technologies. Diyarbakır ,TURKEY
cilgin_erdal@hotmail.com.tr.

INTRODUCTION

A novel and renewable alternative fuel that is simple to obtain, has qualities similar to standard diesel fuel, and does not endanger the environment or living creatures. Biodiesel fuels can be an alternative to traditional diesel fuel because of these characteristics. Biodiesel is a form of fuel that can be made from either vegetable or animal sources. It is biodegradable, non-toxic, and has a better combustion emission profile than petroleum derivatives because it is sourced from renewable resources. It is not a new practice to use vegetable oils in diesel engines. Rudolf Diesel used peanut oil to carry out this application at the beginning of the 18th century. The extensive use of vegetable oils could not be initiated at the time due to the abundance of petroleum, which was cheaper than vegetable oils and had certain limitations with its usage. Oil crops and oil seeds, waste frying oils, and animal fats are all biodiesel manufacturing supplies that have a current commercial worth. Biodiesel is a low-emission fuel that is biodegradable, non-toxic, and environmentally beneficial (Krawczyk, 1996). Biodiesel does not enhance the greenhouse effect because it transforms CO_2 through photosynthesis and speeds up the carbon cycle because it is made from agricultural plants. When left in water for 28 days, 95 percent of biodiesel dissolves, but in diesel fuel, the rate lowers to 40 percent. The quantity of sulfur in biodiesel fuel is substantially lower than diesel, which is considered environmentally favorable because microorganisms can quickly digest it. If biodiesel is used instead of diesel, undesirable environmental effects such as acid rain are avoided. There is a decrease in CO, PM, HF, and SO_x

emissions and an increase in NO_x and HC emissions when pure biodiesel and diesel-biodiesel mixtures are used. With the use of pure biodiesel, sulfur emissions can be fully removed. Hydrocarbon (HC) carbon monoxide (CO) and particle emissions are significantly reduced by biodiesel fuel mixes, whereas nitrogen oxide (NO_x) emissions are marginally increased (Caresana, 2011, Szybist, 2007). Biodiesel fuel mixes with a high O_2 content lower HC and CO emissions by allowing for a cleaner and more thorough combustion (Ghobadian, 2009, Sharon, 2012). In addition, biodiesel fuel blends have a high cetane number, which minimizes combustion time and HC emissions. Behçet et al, Biodiesel is a type of biofuel made from vegetable and animal waste oils. In their work titled "Use as Fuel in a Single Cylinder Diesel Engine," they synthesized fish oil methyl ester and waste cooking oil methyl ester from fish oil and waste frying oil using a transesterification process.

The effects of methyl esters as a fuel in diesel engines were then compared to the impacts of normal diesel fuel on engine performance and exhaust pollutants. Fish oil methyl ester and waste oil methyl ester produced more beneficial exhaust emissions in diesel fuel, according to the test results. They claimed that fish oil methyl ester and waste frying oil methyl ester can be used as a diesel fuel substitute since they emit less HC and CO have superior combustion characteristics, and have positive environmental impacts. Çılğın and İlkılıç, In their study titled Investigation of the effect of microalgae methyl ester on engine performance and exhaust emissions in a diesel engine, they observed a decrease in engine torque and effective engine power

compared to diesel fuel, and an increase in fuel consumption with the use of biodiesel. They also reported that NO_x and O_2 emission values were higher than diesel fuel. HC, CO_2 and CO emissions remained at lower levels in microalgae biodiesel blends. They reported that microalgae methyl ester mixtures in engine emissions are less harmful to the environment. In this study, oil was obtained from Salvia Candidissima plant mass by hydrodistillation and converted to biodiesel by transesterification method. The obtained bio fuel was mixed with standard diesel fuel (B-0) at a rate of 20% (B-20) by volume. B-20 and B-0 fuels were tested in a diesel test engine.

1. Plant Botanical Properties

Lamiaceae family is widespread in the world with 236 genera and 7133 species [9]. Plants belonging to the Lamiaceae family are distributed in high altitude plains in tropical and temperate regions where the climatic conditions of the Mediterranean Region are dominant. Our country, which contains 45 genera, 558 species and 742 taxa of this family, is one of the important gene centers. Endemism is 42.2% (Koyuncu, 2010). Because they are high in essential oils and secondary chemicals, many of the plants in this family are particularly useful in many sectors, including medicine (Kahraman, 2009). The genus Salvia L. known as "sage" in our country, is one of the important medicinal plants widely cultivated in the world. The genus Salvia includes about 1000 species (Özler, 2013). In our country, it has been reported that the number of species has reached 95 (Celep, 2009). Salvia species are important in terms of

both medicine and economy, and are consumed in different ways against different ailments among the public. It also has an important place in the Flora of Turkey and its endemism rate is quite high. Salvia species include annual, perennial and biennial plants in the form of shrubs. Salvia candidissima subsp. Candidissima species is also a perennial plant that can grow up to 60 cm in height and loves different habitats such as rocky limestone and schist slopes and bushes. Members of Lamiaceae, including the genus Salvia, are rich in secondary metabolites. Determining the contents of Salvia species, which have such a rich content and medical importance, is important for the enlightenment of these plants. For this reason, many studies have been carried out both in the world and in Turkey to determine the essential oil compositions and secondary components of Salvia species and are still continuing.

2. MATERIAL METHOD

2.1 Distillation Method

It is a traditional method widely used in obtaining volatile compounds. In small-scale production, the distillation process with a Clevenger type apparatus is carried out in large distillation boilers in industrial applications. The basis of the method; It is based on the boiling of water and plant material for 2-8 hours in a glass balloon connected with the cooler, condensing the oil molecules moving together with the water vapor in the cooler and separating them from the water. The amount of essential oil obtained is expressed volumetrically. Water distillation works best with powdered materials (Linskens, 1997).

Although the amount of oil obtained is high, the high temperature applied during the boiling of water causes some thermal reactions. As a result, artifact formation, hydrolysis and isomerization events occur. Figure 1 shows a thermal degradation that occurs with the effect of temperature and is frequently encountered in distillation methods. Although the composition of essential oils varies depending on the pH, the pH value of the liquid is generally not controlled in the water distillation method (Fakhari, 2005). The distillation scheme is presented in figure 2.

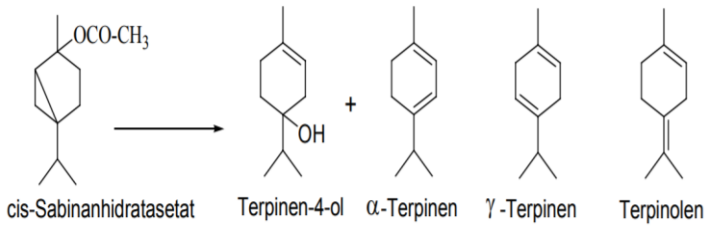

Figure 1: Thermal degradation of sabinanhydracetate (Rowe, 1989).

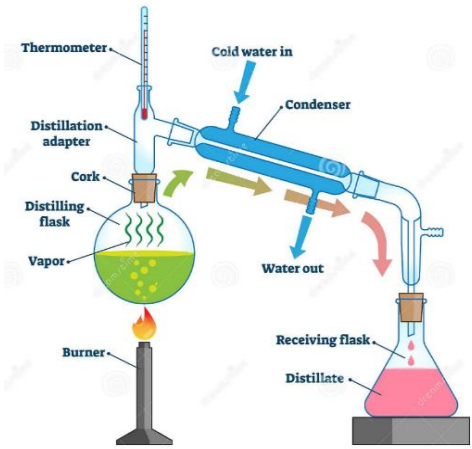

Figure 2: Distillation scheme (https://www.dreamstime.com/distillation)

2.2. Transesterification

It is the most important chemical method followed in the adaptation of vegetable oils as an alternative to petro-diesel fuel. Transesterification is the reaction of vegetable oil with a low molecular mass alcohol in the presence of a catalyst to form glycerine and fatty acid esters. This method is the most effective in reducing viscosity. As a result of this reaction, biodiesel is obtained. The transesterification reaction is as follows. With this method, the following process steps are followed in the production of biodiesel.

Mixing alcohol and catalyst: Sodium hydroxide (caustic soda) or potassium hydroxide is used as catalyst. The catalyst is dissolved in alcohol using a standard mixer.

Reaction: Vegetable or animal oil is added to the alcohol/catalyst mixture in a closed reaction tank. To prevent alcohol leakage, the system is then totally sealed off from the outside world. To speed up the reaction, the reaction mixture is kept at a specific temperature, and the reaction occurs. The recommended reaction duration is 1 to 8 hours, and some systems require the reaction to be carried out at room temperature. The amount of water and free fatty acids in animal or vegetable oils in the diet should be carefully monitored. Soap manufacture and downstream separation of the glycerine by-product can be hampered by high quantities of free fatty acids or water.

Separation: Glycerin and biodiesel are the two main products after the reaction is finished. Each contains a substantial amount of methanol

that was not used in the reaction. At this point, the reaction mixture may be neutralized if necessary. Because the glycerine phase has a far higher density than the biodiesel phase, gravity can easily separate the two phases, allowing the glycerine phase to be easily retrieved from the bottom of the settling vessel. Centrifuges are sometimes used to separate these two components more quickly.

Removal of alcohol: Excess alcohol in each phase is removed by a flash evaporation or distillation procedure after the glycerin and biodiesel phases are separated, and the reaction mixture is neutralized. The ester and glycerine phases are separated. A distillation column is utilized in both circumstances to recover and reuse the alcohol. Water must not be present in recovered alcohol.

Glycerin neutralization: The unused catalyst in the glycerine byproduct is transported to the storage tank to be kept as crude glycerine. In some circumstances, the salt produced during this phase's recovery is recovered and used as fertilizer. The salt is frequently left in the glycerine. Water and alcohol are removed to yield 80-88 percent pure glycerine that can be sold as crude glycerine. Glycerin is distilled to a purity of 99 percent or higher in more complex procedures and marketed to the cosmetics and pharmaceutical industries.

After separating from glycerine, biodiesel is progressively washed with warm water to remove leftover catalyst and soaps, then the water is removed and the biodiesel is transferred to storage. This stage isn't required in some processes. This is usually the last step in the

manufacturing process, and the result is a light amber-yellow liquid with a viscosity similar to diesel. Biodiesel is distilled in some methods to eliminate contaminants. Figure 3 depicts the transesterification reaction, whereas Figure 4 depicts the biodiesel synthesis process flow diagram.

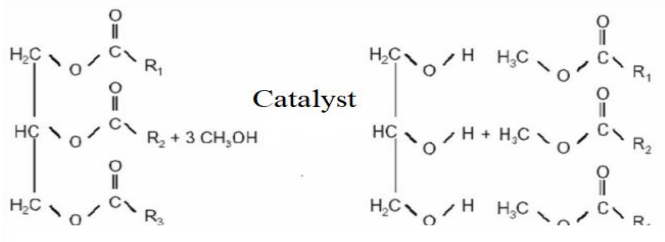

Figure 3: Transesterification scheme

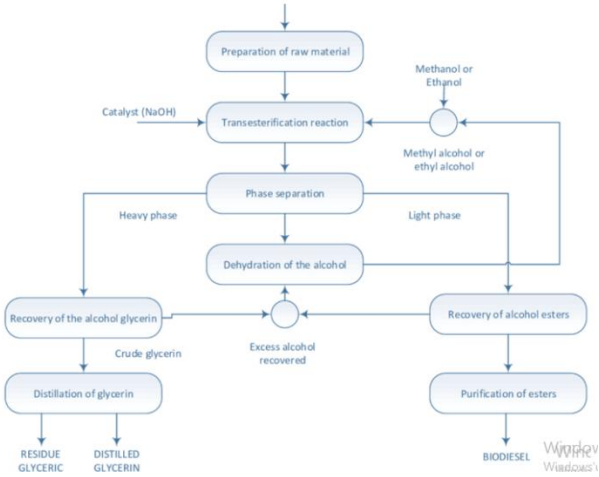

Figure 4: Production process flow diagram of biodiesel (Source:http://www.agencia.cnptia.embrapa.br/.Visited 10/09/2013).

2.6 Test Setups

The constant engine speed for all fuel mixtures is 1500 rpm. Variable engine loading (25%, 50% 100%) was used. A single-cylinder four-stroke compression-ignition direct injection diesel engine was used to perform the experiments (Figure 5). Engine specifications are shown in Table 1.

Table 1: Technical specifications of the test engine

Engine Brand and Type	Kirloskar TV1
Total displacement	0.661 liter
Compression ratio	17.5:1
Bore	87 mm
Stroke	110 mm
Start of injection	0-25° bTDC
Connecting rod length	234 mm
Maximum power	3.5 kW @ 1500 rpm

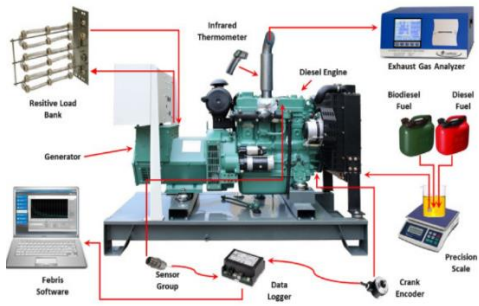

Figure 5. Schematic view of the experimental setup (Aydın, 2020).

3.EXPERIMENTAL RESULTS

3.1. Carbon Monoxide Emission (CO)

The formation of CO is due to the incomplete oxidation of the fuel in the combustion chamber and the low temperature of the burnt gas. In addition, turbulence density is another important parameter affecting CO emissions, since it is effective in the formation of homogeneous mixtures. Figure 6 shows the variation of CO emissions depending on engine load. The highest CO emission values were obtained with B-0 fuel at all loads. As the amount of fuel injected into the cylinder increases depending on the load, the high temperature in the combustion chamber ensures complete combustion, and the CO emissions decreased in both fuels. The oxygen (O_2) contained in B-20 fuel improves combustion. Therefore, the lowest CO emission values in all load conditions were obtained with B-20 fuel.

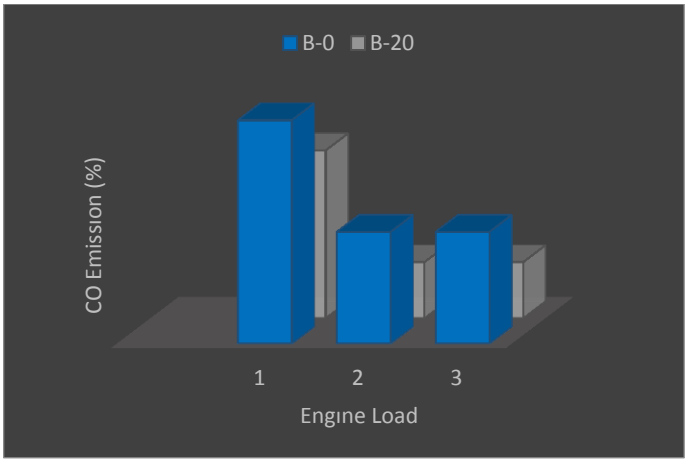

Figure 6: CO Emission changes

3.2. Nitrogen Oxide Emission (NO_x)

Nitrogen (N_2) and oxygen (O_2) combine at temperatures above 1800 K and cause NOx formation. Maximum pressure at high loads as the air/fuel ratio increases in diesel engines. therefore, increasing the maximum temperature ensures that the mixture burns in a wider region at a value close to the stoichiometric ratio. In this case, NO_x formation increases. Reducing the air/fuel ratio reduces NO_x emissions. However, this decrease is not higher in diesel engines due to the inability to properly spray the fuel (Heywood, 1998). The shortening of the ignition delay time will reduce the amount of fuel accumulated in the combustion chamber, and therefore the temperature increase in the flash combustion period, especially when high cetane number fuels are used, thus reducing NO_x emissions. In addition, parameters such as turbulence rate, injector nozzle hole number, combustion chamber design, injection pressure, which are effective in the formation of the mixture in diesel engines, are important in NO_x formation (Challen, 1999). Figure 7 shows the variation of NO_x emissions depending on engine load. The most important problem of biodiesel fuels obtained from vegetable oils is the high NO_x emission after combustion. The formation of NO_x is due to high gas temperatures at the end of combustion, oxygen in the fuel content, and rapid oxidation reactions (Heywood, 1988). The main reason for high NO_x emission in a diesel engine using biodiesel fuel is the oxygen concentration in the fuel. Therefore, oxidation reactions occur rapidly during the combustion process and high gas temperatures are obtained in the combustion chamber. Thus, NO_x

emissions increase (Palash, 2013, Uyumaz, 2018). When Figure 7 is examined, the amount of energy injected into the cylinder increases with the increase of engine load, and NO_x emissions increase depending on the increase in the end-combustion gas temperatures. The highest NO_x emission was obtained with the use of biodiesel fuels.

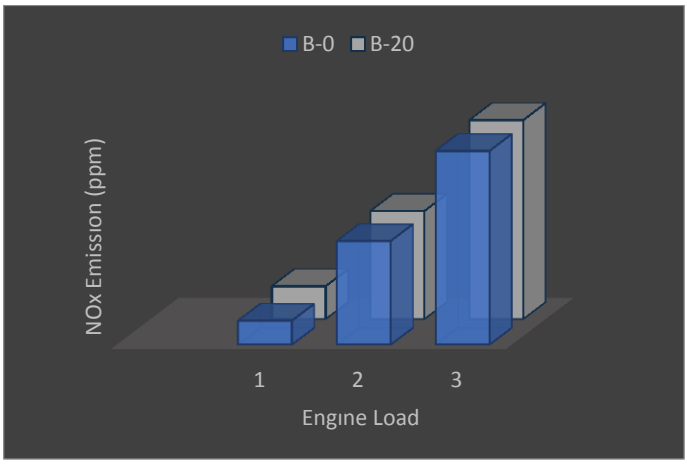

Figure 7: NOx Emission changes

3.3. Hydrocarbon Emissions (HC)

HC emissions, another harmful exhaust emission from vehicles, are caused by the fuel not participating in combustion and evaporation in the fuel system. HC emissions have toxic properties and have been considered carcinogenic for many years (Pulkrabek, 2010). The most important HC formation mechanisms are the filling of the cavities in the combustion chamber with the air-fuel mixture, the absorption and desorption of the fuel into the oil layer, the liquid fuel remaining in the cylinder, the leaks in the valve bearing cavities and the cold operating

conditions (Nam, 2008). The flame advancing in the combustion chamber can go out when it comes into contact with the cold cylinder walls. In the meantime, oxidation reactions in the cylinder walls deteriorate, combustion cannot be completed and HC is released. When the HC changes are examined in Figure 8, the oxygen content of B-20 fuel increased oxidation, causing HC emissions to be lower compared to B-0 fuel. Çığın, stated that he found similar results in the study in which the salvia plant rained with a volumetric% mixture ratio.

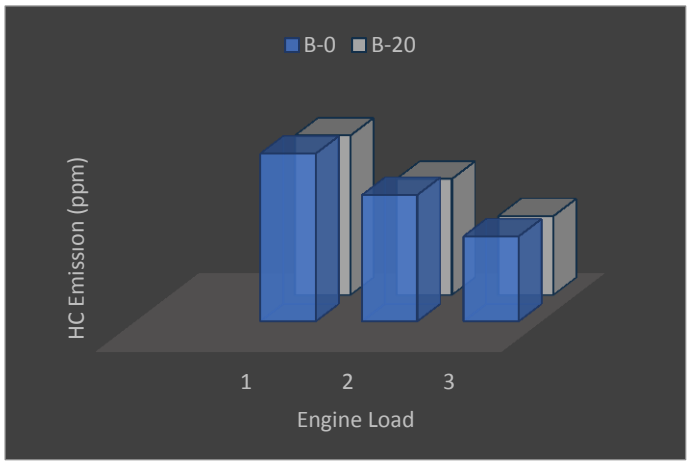

Figure 8: HC Emission changes

3.4.Carbon Dioxide Emission (CO_2)

With the decomposition of the carbon and hydrogen components in the fuel during combustion, the hydrogen component turns into water. The carbon component, on the other hand, turns into CO_2 if it finds enough oxygen during oxidation, and turns into CO or smoke if it cannot find it. Figure 9 shows the relationship between the CO_2

concentrations of the test fuels and the engine load. Experimental results show that CO_2 concentrations increase with the use of B-20 fuel compared to B-0 fuel. CO_2 emissions are the result of B-20 fuel oxygen ratio improving combustion.

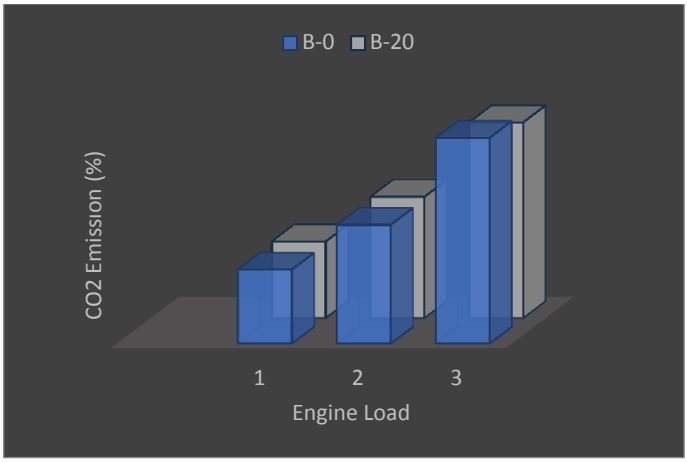

Figure 9: CO_2 Emission changes

3.5. Specific fuel consumption variation (SFC)

Specific fuel consumption refers to the mass of fuel consumed to produce 1 kW of power. In the literature review, it is generally stated that SFC is higher in biodiesel blended fuels than in diesel fuel. This increase is due to the lower heating values of biodiesel blended fuels than diesel fuel. For this reason, the amount of fuel consumed per unit power is higher since the heating values of biodiesel blended fuels are low (Çılğın, 2015). However, in this study, the use of B-20 fuel decreased SFC compared to B-0 fuel. This phenomenon is the addition of oxygen in the biodiesel content, which promotes combustion, and the higher calorific value than diesel fuel.

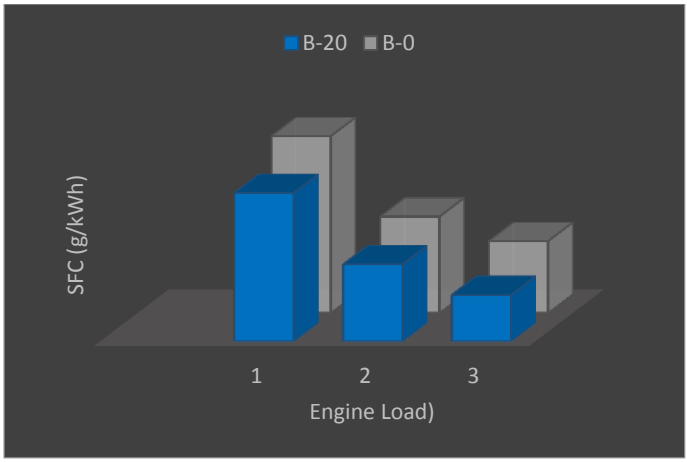

Figure 10: Specific fuel change

4. COMBUSTION PARAMETERS

4.1. Cylinder pressure variation

In Figure 11-12-13-14, the changes in the cylinder pressure change and heat release values of the test fuels depending on the load are given. By loading the engine for both test fuels, both cylinder pressures and heat release values increased. Because the fuel taken in with loading increases and high temperatures and pressure are created during combustion.

When Figures 11,12,13,14 were examined, it was seen that higher values were obtained with B-20 fuel compared to B-0 fuel. The heat evaporation of B-20 fuel is higher than B-0 fuel; This feature provides cooling of the fuel-air charge and increases the density of the load. This results in higher CP and HRR output. In addition, the addition of Biodiesel to B-0 fuel increases the ignition delay; therefore more fuel accumulates in the premixed combustion stage and is the reason for

faster combustion. therefore, the peak pressure and heat release values increase. Çılgın, reported an increase of 4.99% in the pressure values of the fuel in his study with salvia.

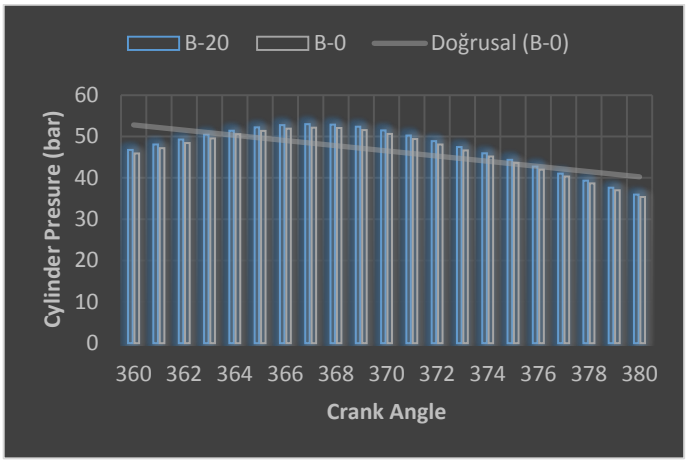

Figure 11: Cylinder pressure variations

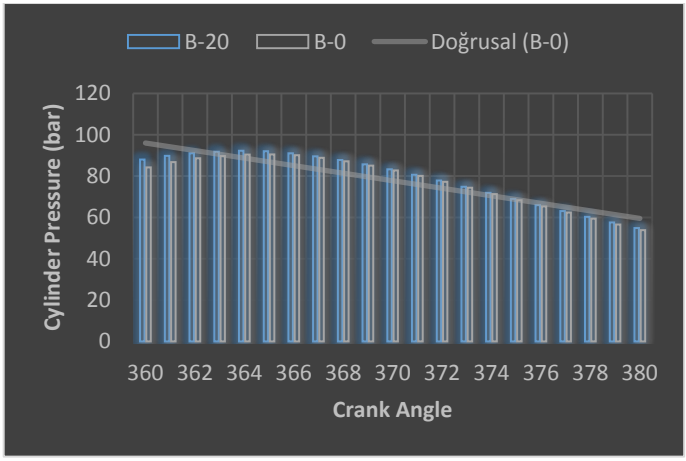

Figure 12: Cylinder pressure variations

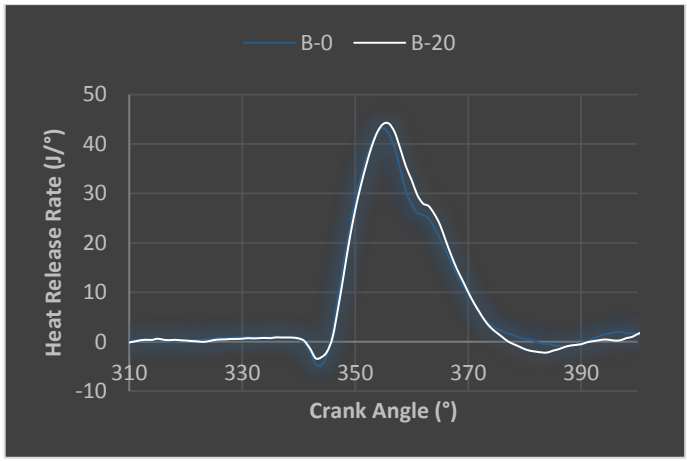

Figure 13: Net heat release changes

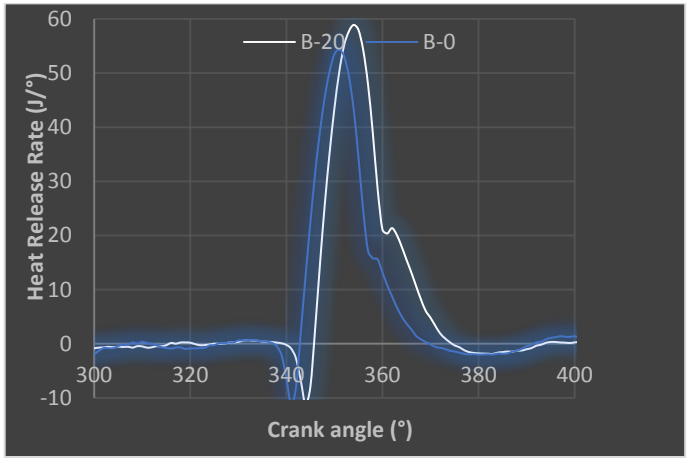

Figure 14: Net heat release changes

4.2. Cumulative Heat Dissipation

Figure 15-16. shows the variation of the cumulative heat dissipation depending on the crank angle. The cumulative heat distribution can be expressed as the sum of the heat energy released in the combustion chamber depending on the crank angle (Aksoy, 2019). In addition,

analysis can be made about the combustion stages of the mixture by normalizing the cumulative heat distribution. It was observed that higher cumulative values occurred with the use of B-20 fuel at all engine loads compared to B-0 fuel. This is due to the high oxygen content and high thermal energy of biodiesel.

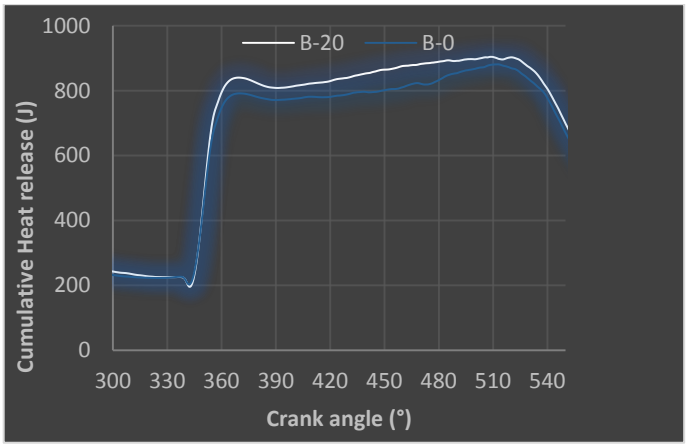

Figure 15: Net heat release changes

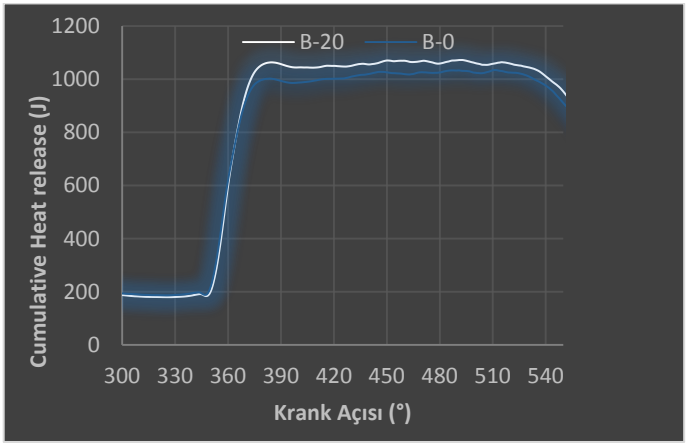

Figure 16: Net heat release change

CONCLUCSION

In this study, Salvia Candidissima plant was investigated as a different new and renewable biodiesel source. First of all, oil was obtained from the plant Salvia Candidissima by hydrodistillation. Biofuel was produced by applying the transesterification procedure to the obtained oil. The produced biofuel diesel blends and reference diesel fuel were tested in a diesel test engine. As a result of the test, the data presented below were obtained. With the use of mixed fuel (B-20), NO_x and CO_2 data, which are exhaust emissions, increased, while CO and HC emissions decreased. In the combustion data, it was observed that the mixed fuel formed higher values for all of the CP, HRR and CHR values. In line with these results, it can be said that B-20 fuel provides significant overall improvements in the diesel engine combustion process.

REFERENCES

Aydın, S. Comprehensive analysis of combustion, performance and emissions of power generator diesel engine fueled with different source of biodiesel blends. Volume 205, 15 August 2020, 118074. Energy

Aksoy, F. Yılmaz, E. (2019). %10 Balık Yağı Biyodizeli-%90 Dizel Yakıt Karışımı İle Çalışan Direkt Enjeksiyonlu Bir Dizel Motorunda Yanma ve Performans Karakteristiklerinin İncelenmesi. GU J Sci, Part C, 7(1): 12-24 (2019)

Behçet, R. Aydın, S. Çakmak, A. (2012). Bitkisel ve Hayvansal Atık Yağlardan Üretilen Biyodizellerin Tek Silindirli Bir Dizel Motorda Yakıt Olarak Kullanılması. Iğdır Üni. Fen Bilimleri Enst. Der. / Iğdır Univ. J. Inst. Sci. & Tech. 2(4): 55-62, 2012

Caresana, F. (2011).Impact of biodiesel bulk modulus on injection pressure and injection timing. The effect of residual pressure. Fuel 2011;90:477–85.

Celep, F. Doğan, M. Duran, A. (2009). A new record for the flora of Turkey: Salvia viscosa Jacq.(Labiatae). Türkish Journal of Botany, 32: 57-60

Challen, B. Baranescu, R. (1999). Diesel Engine Reference Book 2nd ed. Butterworth-Heinemann, Oxford, 479- 480.

Çılğın, E. (2012). Investigation of the usability of essential oils in diesel engines as a new biodiesel source. GÜFBED/*GUSTIJ* (2021) 11 (2): 573-585

Çılğın, E. (2015). 3. Nesil Biyoyakıt Teknolojisi Alglerin bir Dizel Motorunda Performans ve Egzoz Emisyonlarına Etkisinin Araştırılması. Iğdır Üni. Fen Bilimleri Enst. Der. / Iğdır Univ. J. Inst. Sci. & Tech. 5(3): 33-41, 2015

Çılğın, E. (2020). Investigation of the Usability of Essential Oils as Fuel in Diesel Engines. Dicle University Journal of Institute of Natural and Applied Science DUFED, *9 (2) (2020) 35-50*

Çılğın, E. İlkılıç, C. (2015). Mikroalg metil esterinin bir dizel motorunda, motor performansı ve egzoz emisyonlarına etkisinin araştırılması. Erciyes Üniversitesi Fen Bilimleri Enstitüsü Dergisi, 31(1):68-72

Fakhari, A. (2005). Hydrodistillation-Headspace Solvent Microextracti On, A New Method For Analysis Of The Essential Oil Components Of Lavandula angustifolia Mill. J.of Chromatography A, 1098, 14-18

Ghobadian, B. Rahimi. H. Nikbakht, A.M. Najafi, G. Yusaf, T.F. (2009). Diesel engine performance and exhaust emission analysis using waste cooking biodiesel fuel with an artificial neural network. Renewable Energy 2009;34:976–8

Harley, RM. Atkins, S. Budantsev, A. Cantino, PD. Conn, BJ. Grayer, R. Harley, MM. (2004). Labiatae. In: Kubitzki, K. (ed.), The Families and Genera of Vascular Plants, vol. 7, pp. 167-275. Springer-Verlag, Berlin

Heywood, J. B. (1988). Combustion in compressionignition engines. Internal combustion engine fundamentals, Mcgraw-hill, New York

Heywood, J.B. (1998). Internal Combustion Engines Fundamentals. McGraw-Hill, NewYork, 504-541.

Kahraman, A. Celep, F. Doğan, M. (2009). Morphoogy, anatomy and palynology of Salvia indica L.(Labiatae). World Applied Sciences Journal, 6 (2):289-296

Koyuncu, O. Yaylacı, ÖK. Öztürk, D. Erkara, İP. Savaroğlu, F. Akçoşkun, Ö. Ardıç, M. (2010). Risk categories and ethnobotanical features of the Lamiaceae taxa growing naturally in Osmaneli (Bilecik/Turkey) and environs. Biological Diversity and Conservation, 3(3): 31-45

Krawczyk. T. (1996). Biodiesel-alternative fuel makes inroad but hurdles remain. Inform 1996;7: 801- 5.

Linskens, H.F. Jackson, J.F. (1997). Modern Methods of Plant Analysis, Vol. 19: Plant Volatile Analysis, Springer, Germany..

Nam, E. Scarbro, C. (2008). Analysis of Particulate Matter Emissions from Light-duty Gasoline Vehicles in Kansas City. USA Environmental Protection Agency, 6-7

Özler, H. Pehlivan, S. Celep, F. Doğan, M. Kahraman, A. Fişne, AY. Başer, B. Bagherpour, S. (2013). Pollen morphology of Hymenosphace and Aethiopis

sections of the genus Salvia (Lamiaceae) in Turkey. Turkish Journal of Botany, 37:1070-1084

Palash, S. M. Kalam, M. A. (2013). Impacts of biodiesel combustion on NOx emissions and their reduction approaches, Renewable and Sustainable Energy Reviews, Cilt. 23, s. 473-490. DOI: 10.1016/j.rser.2013.03.003

Pulkrabek, W.W. (2010). Engineering Fundamentals of The Internal Combustion Engine. Prentice Hall, New Jersey

Rowe, J.W. (1989). Natural Products of Woody Plants Vol.2, Springer, Germany

Sharon, H. Karuppasamy, K. Soban Kumar, D.R. Sundaresan, A. (2012). A test on DI diesel engine fueled with methyl esters of used palm oil. Renewable Energy 2012;47:160–6.

Szybist, J.P. Song, J. Alam, M. Boehman, A.L. (2007). Biodiesel combustion, emissions and emission control. Fuel Processing Technology 2007;88:679–91.

Uyumaz, A. (2018). Combustion, performance and emission characteristics of a DI diesel engine fueled with mustard oil biodiesel fuel blends at different engine loads. Fuel, Cilt. 212, s. 256-267. DOI: 10.1016/j.fuel.2017.09.005

CHAPTER 2

INVESTIGATION OF MENNTHA TOMENTOSA OIL IN BIOFUEL RESOURCE RESEARCH

Assoc. Prof. Dr. Erdal ÇILĞIN[1]

[1]Dicle University Technical Sciences Angel School, Department of Motor Vehicles and Transportation Technologies. Diyarbakır, TURKEY
cilgin_erdal@hotmail.com.tr.

INTRODUCTION

One of the biggest problems in front of the world is the energy resources that will run out. The cause of many international problems, the main element of many balances, oil will run out in the 21st century. Oil, which is the raw material for at least 3,000 products directly and indirectly for thousands of products, is running out and is a matter of global concern. In addition, these products have many harms to nature and the environment at every stage, from the underground extraction to the processing and placing on the market under various names. These disadvantages have encouraged researchers to research and use alternative and renewable fuels (Xue, 2014). Among the alternative sources found at the end of these studies, the most prominent source for diesel engines is biodiesel. Biodiesel is derived from biological sources such as oilseeds and animal fats. Biodiesel is defined as a fuel containing mono-alkyl esters of long chain fatty acids (Canakci,2001). Biodiesel provides improvements especially in exhaust emissions such as CO and HC. Biodiesel is generally produced from fixed vegetable oils such as Palm oil, Sunflower oil, Sesame oil, Rapeseed oil, as well as waste cooking oils. Today, in many countries around the world, agricultural areas are reserved for oilseed crops to obtain these oils. Separation of agricultural lands for biodiesel resource cultivation has created serious problems in food production. In addition, the edibility of some oilseed crops (cotton, soybean, rapeseed, safflower, etc.) is another aspect of the problem. What is revealed in the sum of these negativities is that inedible plants and vegetable oils are a source of biodiesel instead of

oilseed plants (Duren,2015). In this study, different from the fixed oils (olive oil, soybean, cotton, canola, etc.) used until now, essential oils were preferred. Essential oils are mixtures produced from parts of plants or plant sources such as roots, stems, leaves, fruits, bark and flowers (Yaylı,2013). Menntha tomentosa with 6-7 ml oil content in 100 grams' dry mass was used as essential oil plant. Menntha tomentosa is a perennial wild plant that is generally not a selective plant and can adapt to most climatic conditions. This plant grows in almost every region of Turkey. It is a naturally grown plant that is not consumed for human and animal food.

1. FIXED AND ESSENTIAL OILS

1.1. Fixed Oils

The storage material of plants and animals is called fixed oil. They can be mostly liquid, sometimes solid. As the name suggests simply, these oils are not volatile. The most well-known examples of fixed oils are Olive Oil and Sunflower oil. They are insoluble in water. They are obtained by cold or hot pressing method or by using some solvents. Most of the fixed oils from the lipid group are composed of glycerides. Other substances found in fixed oils are wax, sterols, phosphatides, fat-soluble vitamins, aliphatic alcohols, hydrocarbons and kaolinites [6]. Olive Oil, Black Cumin Oil, Linseed Oil, Walnut Oil, Almond Oil, Sesame Oil, St. John's Wort Oil are examples of fixed oils. Fixed oils are used as a source of biodiesel.

1.2. Essential Oils

Essential oils are usually colorless or light yellow, volatile, strong-smelling and volatile oils, produced from parts of plants or plant sources such as roots, stems, leaves, fruits, bark, flowers, which are liquid at room temperature, sometimes freeze, easily crystallize. are oily mixtures (Yaylı,2013). There are terpenic or non-terpenic components in the composition of essential oils. These are hydrocarbons and their oxygenated derivatives. Some components may contain nitrogen or sulfur. It exists in compounds found in alcohol, acid, ester, epoxide, aldehyde, ketone, amine, sulfite and forms (Başer,1998).

2. MATERIALS AND METHODS

2.1. Materials

Menntha tomentosa is a Lamiaceae family perennial herb. It grows wild in practically every region of Turkey, earning it the nicknames punk and pune among the locals. Menntha tomentosa is the scientific name for the plant. Although it prefers a mild and temperate climate, it is also tolerant of hot and dry weather

2.2. Oil Percentage

A Clevenger-type apparatus was used to determine the percentage of pure essential oil of the Menta tomentasa plant. (Fig. 1(a)), A retort was manufactured for mass oil extraction. (Fig. 1(b)). Both the clevenger apparatus and the retort were used for the distillation process. The basis of the method; It is based on boiling water and

plant material for 3-5 hours in a glass balloon connected with the cooler, condensing the oil molecules moving with the water vapor in the cooler and separating them from the water. The amount of essential oil obtained (Figure 1(c)) was obtained as 6-7 ml in 100g dry biomass. Water distillation works best with powdered materials (Linskens, ,1997). Table 1 shows the chemical components of essential oils.

Figure 2: Steps of oil extraction

(a) Copper vessel (retort) (b) Essential oil

Table 1: Chemical and physical properties of the essantıel oil

Peak Number	Retation Time	Constituent	Average Rate(%)
1	12.526	Alpha-Pinene	2.93
2	16.259	Beta-Pinene	6.12
3	16.844	Sabinene	3.29
4	18.686	Myrcene	2.63
5	20.374	Limonene	3.12
6	20.896	1,8-Cineole	52.44
8	31.138	Menthone	5.30
9	32.114	İsomenthone	4.35
10	33.348	Linalool	0.51
13	35.526	Beta-Caryophyllene	10.44
14	37.119	Pulegone	10.98

During the production of Menntha tomentosa methyl ester, a magnetic stirrer with heating, a 2,000 ml flask, and a thermometer with a sensitivity of 0.01ºC were used. In the esterification process, potassium hydroxide was used as catalyst and 99.5% pure methyl alcohol was used as alcohol. The catalyst was dissolved in methyl alcohol and added to the vegetable oil heated to 50ºC. This mixture was stirred at 600 d d-1 at constant 60ºC for approximately one hour. Then, it was taken to the separating funnel and the glycerine was expected to settle to the bottom. After separating the glycerine and methyl ester, the methyl ester was washed with distilled water (Çılğın,2015). The processing steps of the produced Menntha tomentosa oil methyl ester are given (Figure 2).

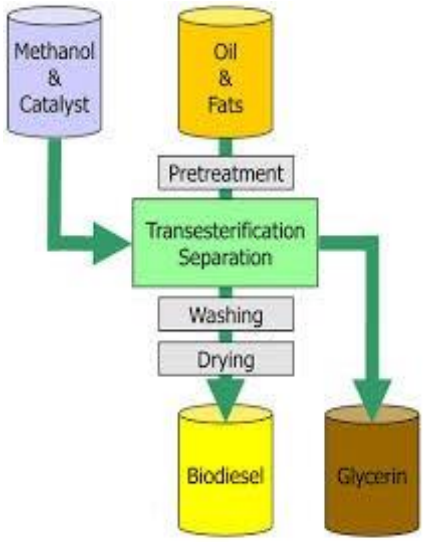

Figure 2: Flow chart of methyl ester production (https://www.slideshare.net/ShivajiThube/process-dynamics)

Menntha tomentosa biodiesel was mixed with pure diesel (BO) fuel in 4 different ratios. The largest volumetric blend was limited to MB-20 (20 vol% biodiesel and 80 vol% diesel fuel). Because MB-20 and lower grade mixes generally do not require engine modification (Mato,2014). For all fuel mixtures, the constant engine speed is 1500 rpm. Varying engine loading (25%, 50%, 75%, 100% at four levels) was used. A single-cylinder four-stroke compression ignition (CI) direct injection diesel engine was used to perform the experiments (Figure 3).

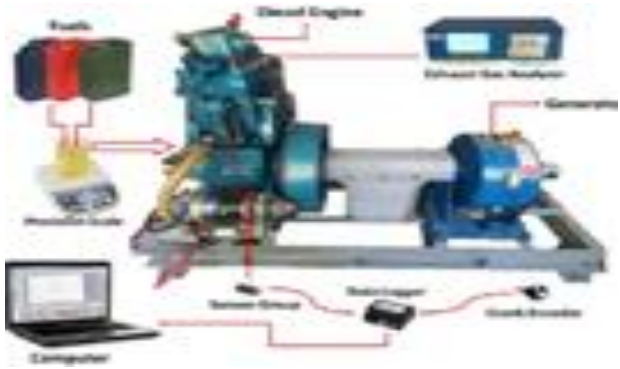

Figure 3: Engine test set-up and instrument (a) real and (b) schematic.

3. EXPERIMENTAL RESULTS

3.1. Engine Emissions

3.1.1. Carbon Monoxide Emissions

CO emission changes are given for experimental fuels at different engine loads.(Figure 4/5.) With the use of mixed fuel samples, carbon monoxide emissions were reduced. Oxygen in the essential oil-based biodiesel content reduced CO, ensuring complete and clean combustion (Sarıdemir,2016). When the biodiesel blend concentration in the blend fuel ratio increased, the CO emissions decreased. The extra oxygen content in the blended fuel samples improved combustion and converted CO to CO_2.Thus, CO emissions for blended fuels were reduced compared to pure diesel (BO) fuel. Compared to pure diesel (BO) fuel, the biggest reduction was 31.25% with MB-20 fuel.

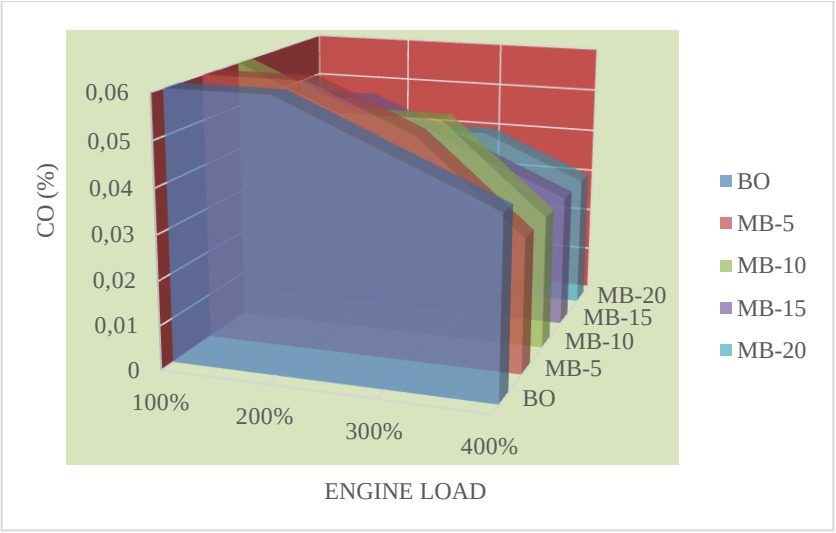

Figure 4: The CO changes obtained depending on the engine load are given.

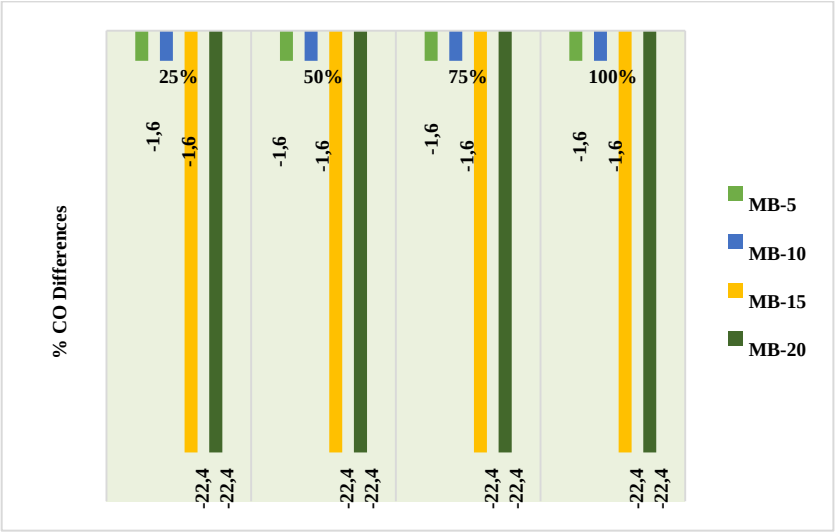

Figure 5: CO change differences

3.1.2 Carbon dioxide Emissions

With the decomposition of the carbon and hydrogen components in the fuel during combustion, the hydrogen component turns into water. The carbon component, on the other hand, turns into CO_2 if it finds enough oxygen during oxidation, and turns into CO or smoke if it cannot find it. The variation of CO_2 concentrations for test fuels at different load conditions is given in figure 6/7. With engine loading, CO_2 concentrations increased for all fuels. It was observed that the CO_2 emission difference increased as the biodiesel ratio in the blended fuel increased. There were increases of 1.14%, 4.59%, 9.19% and 13.79% in MB-5, MB-10, MB-15 and MB-20, respectively. As seen in Figure 6, biodiesel blend fuels reduced CO emissions. Because the amount of oxygen improved combustion and CO_2 emissions increased.

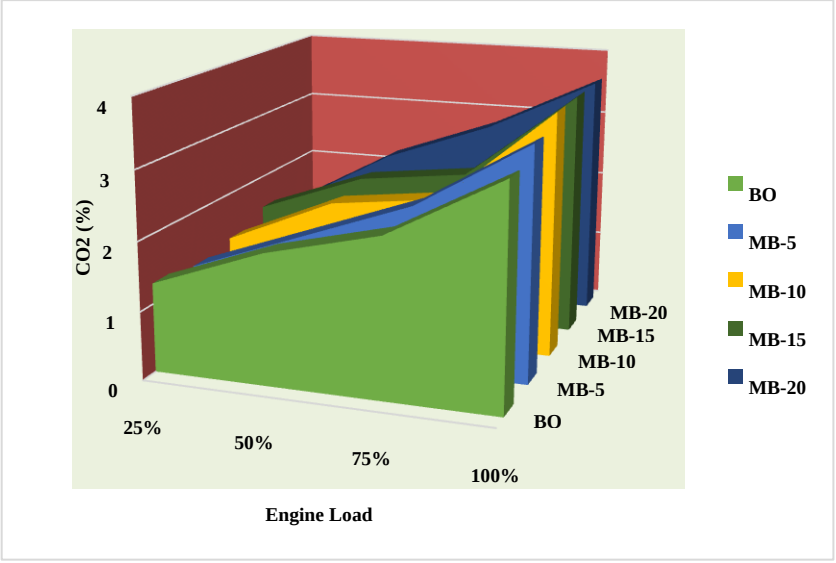

Figure 6: CO_2 changes depending on engine load are given.

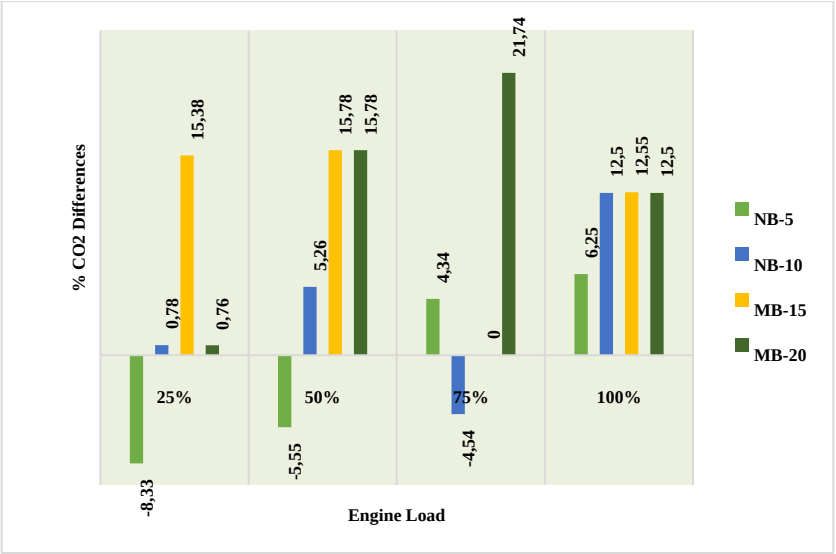

Figure 7: CO_2 Exchange differences

3.1.3 Hydrocarcon emissions

HC emissions occur mostly in regions where combustion is not complete. The two main reasons for the formation of HC are low temperature and insufficient oxygen in the environment. HC changes depending on engine load are given Figure 8/9. HC emissions for all fuels improved with load increase because ambient temperature increased with increasing loads. When fuel changes were examined, HC emissions decreased significantly with the use of mixed fuel compared to pure diesel (BO) fuel. This reduction was 6.13%, 13.07%, 14.56%, 20.13% in MB-5, MB-10, MB-15, MB-20 compared to pure diesel fuel (BO), respectively. This reduction provided by the use of mixed fuel is the same reason as the decrease in CO emissions, which is the product of incomplete combustion. The use of oxygen

additives that support complete combustion is the cause of hydrocarbon reduction (Selvan, 2009).

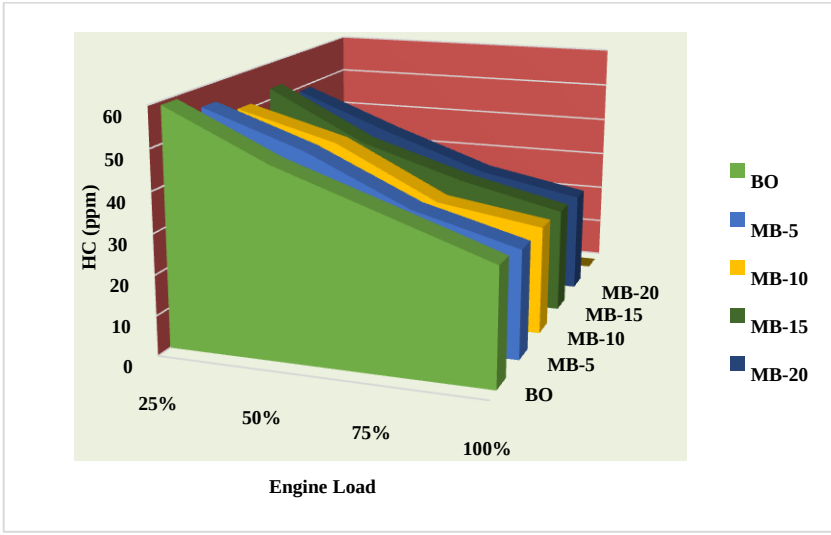

Figure 8: The relationship between engine load and HC for different blends.

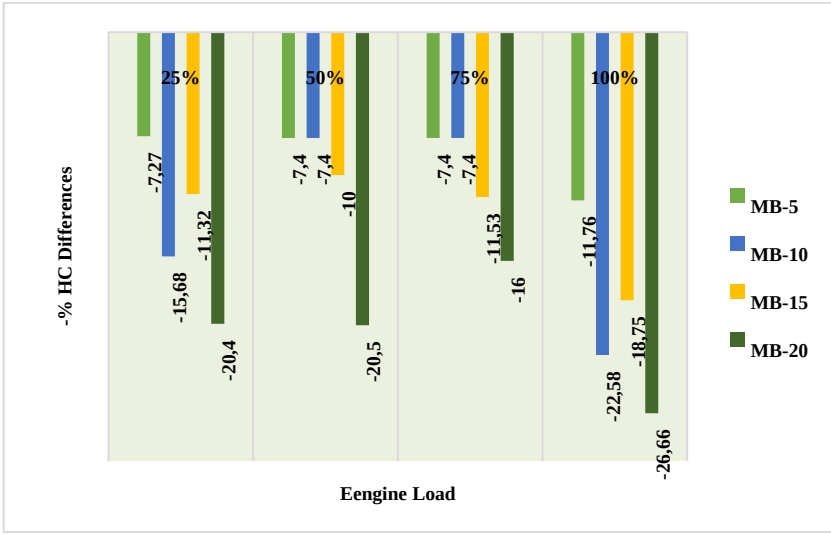

Figure 9: HC changeover differences

3.1.4 Nitrous oxide Emissions

In the combustion process, nitrogen oxides are formed as a result of the combination of nitrogen in the air with oxygen at high temperatures. NO_x contains nitrogen as the main element. When exhaust gases are thrown into the atmosphere and in contact with oxygen, some of the NO turns into NO_2 and other NO_x. Two important parameters affecting NO_x formation are combustion chamber temperature and air/fuel ratio. NO_x changes depending on engine load are given Figure 8. When the emission changes were examined, it was seen that the oxygen content, which reduced the CO and HC emissions, increased the NO_x concentrations. Because oxygen increases combustion temperatures and reduces emissions such as CO and HC, which are products of incomplete combustion. However, NO_x emission, which is a high temperature product, increases with the increase of the combustion temperature of oxygen. Many researchers stated that the use of mixed fuels (pure diesel-biodiesel) increased NO_x concentrations compared to pure diesel (Çelik,2008).

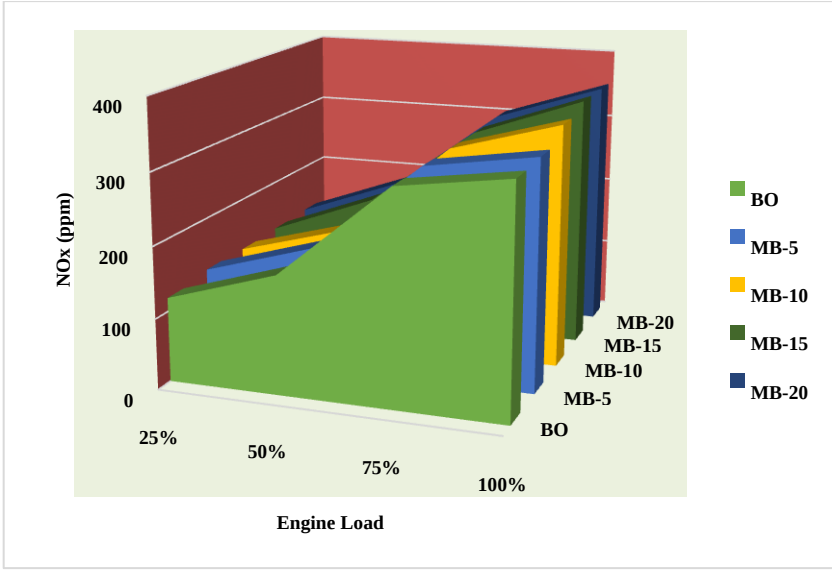

Figure 10: The relationship between engine load and NO_x for different blends.

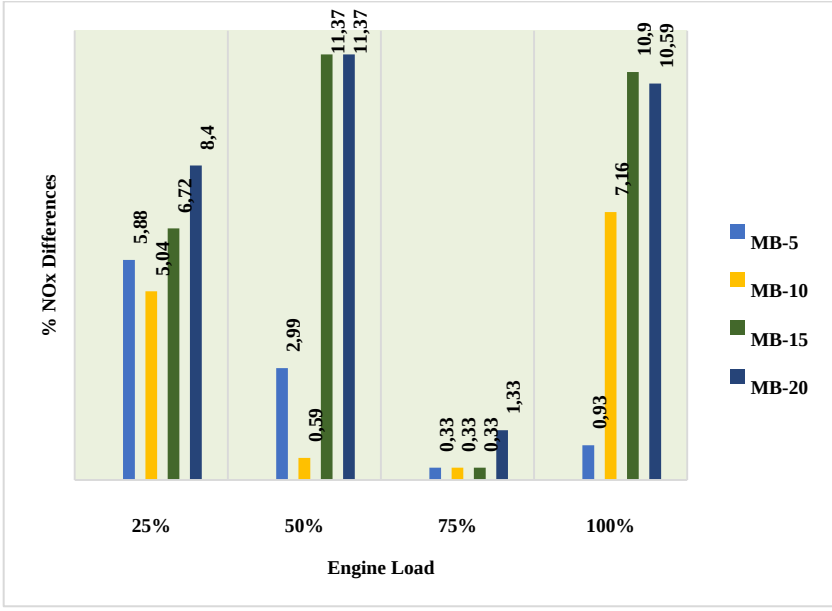

Figure 11: NO_x Changeover differences

3.2. Engine Performance

The following equations (Equation 1, Equation 2, Equation 3, Equation 3) are used in the calculations of Brake specific fuel consumption (BSFC) and Brake thermal efficiency (BTE).

Brake Power (PB) : $\frac{2\pi.N\ [\ W.Re\ .(9.81)]}{60000}$ (1)

Where,

N :Engine speed (rpm)

W :Load applied on the engine

Re :Effective Radius of brake drum

Total Fuel consumption (TFC) : $\frac{5x\ (spcific\ gravity\ of\ fuel)x3600}{t\ x\ 1000}(\frac{kg}{h})$ (2)

t : time for 5cc fuel consumption in seconds

Brake specific fuel consumption (BSFC): $\frac{TFC}{BP}(\frac{kg}{kWh})$ (3)

Brake thermal efficiency (BTE) : $[\frac{BP\ x\ 3600}{TFC\ x\ C_v}]$ x100 (4)

Cv :Calorific value of fuel

3.2.1. Engine performance

Figure 12-17 depicts the impact of test fuels on engine power (kW) and torque (Nm).At all engine loads, increasing the ratio of essential

oil to biodiesel in the blended fuel boosted both engine power and torque.The rise in average effective pressure for blended fuels can be attributed to the power and torque gains in favor of blended fuels (Bayraktar ,2005). Biofuels have a higher enthalpy of evaporation than reference diesel fuel, which cools the fuel-air charge and enhances the load density.As a result, higher engine performance characteristics (kW and Nm) are attained (Çelik,2008). Another reason for the improvement in engine power is that when the percentage of essential oil and biodiesel in the mixed fuel increases, so does the blend fuel density and engine volumetric efficiency (Al-Hasan,2003). The ignition delay (ID) time is increased when essential oil biodiesel is added to the mix fuel; a longer ID causes more fuel to collect in the combustion process. This collected gasoline will burn immediately, resulting in torque and power due to the high pressure (Selvan, 2009). When comparing the torque and power graphs, it was discovered that the greatest differences occurred when using MB-20 fuel against DF fuel.At 25 percent load, the disparities were 17.5 percent, 18.36 percent at 50 percent load, 13.63 percent at 75 percent load, and 10.99 percent at 100 percent load.MB-20 fuel was also used to produce the maximum torque ratings.At 25 percent load, the variances were 8.2 percent, 7.91 percent at 50 percent load, 8.94 percent at.75 percent load, and 7.14 percent Nm at 100 percent load.Another performance parameter is the specific fuel consumption graph (fig.11).The essential oil biodiesel blend fuels had a lower specific fuel consumption than the reference diesel fuel.This is owing to the essential oil biodiesel blend's higher calorific value than the

reference diesel fuel (İlkılıç ,2013). Furthermore, it can be observed from the figures that the SFC reduces as the biodiesel ratio in the blended fuel increases. B-20 was the gasoline with the lowest SFC.While MB-20 gasoline had an SFC of 252 g/kWh, BO had an SFC of 277.25 g/kWh.

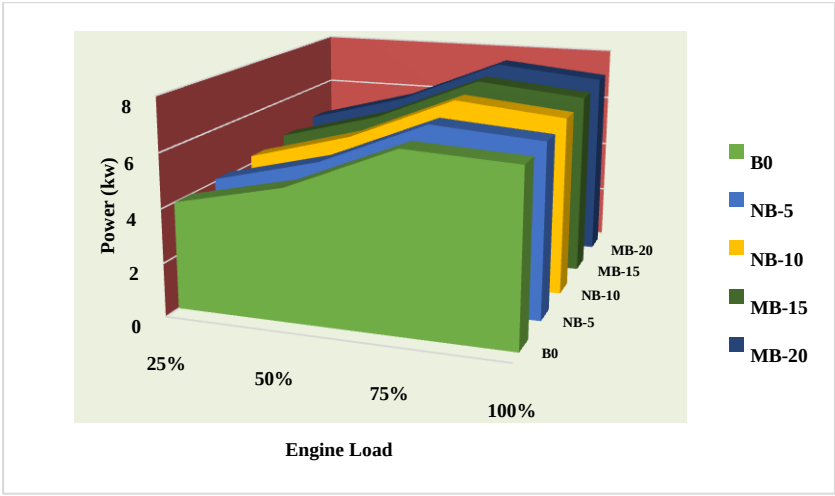

Figure 12: The relationship between engine load and (Power) for different blends.

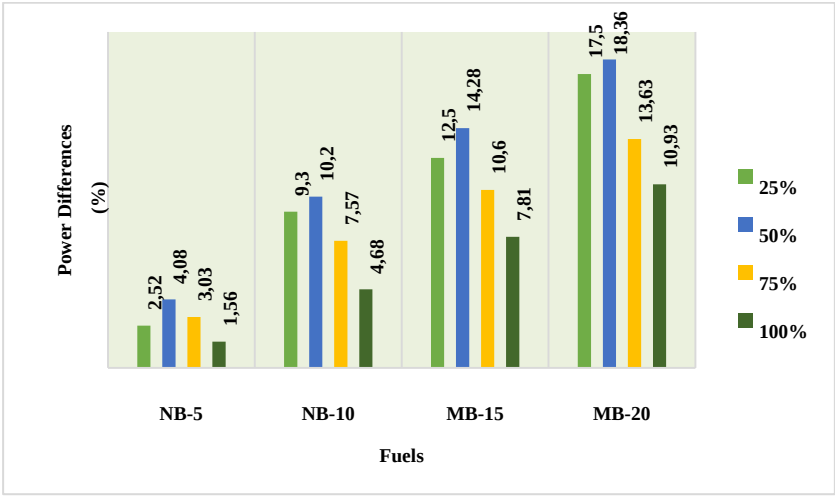

Figure 13: Power variation differences.

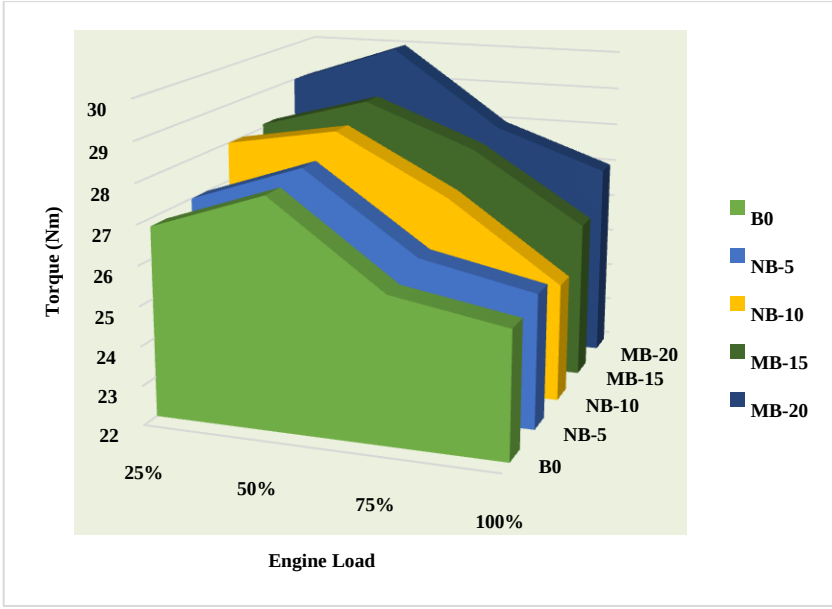

Figure 14: The relationship between engine load and Torque for different blends.

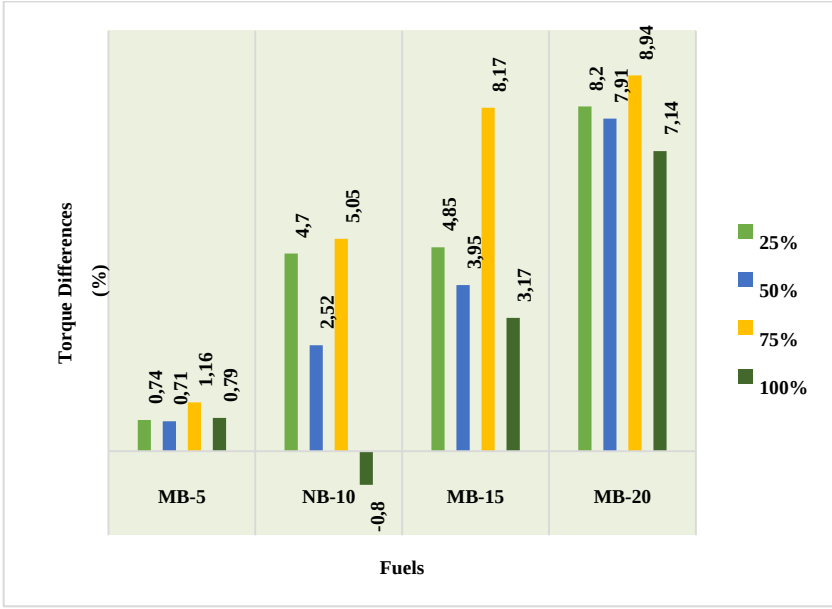

Figure 15: Torque variation differences

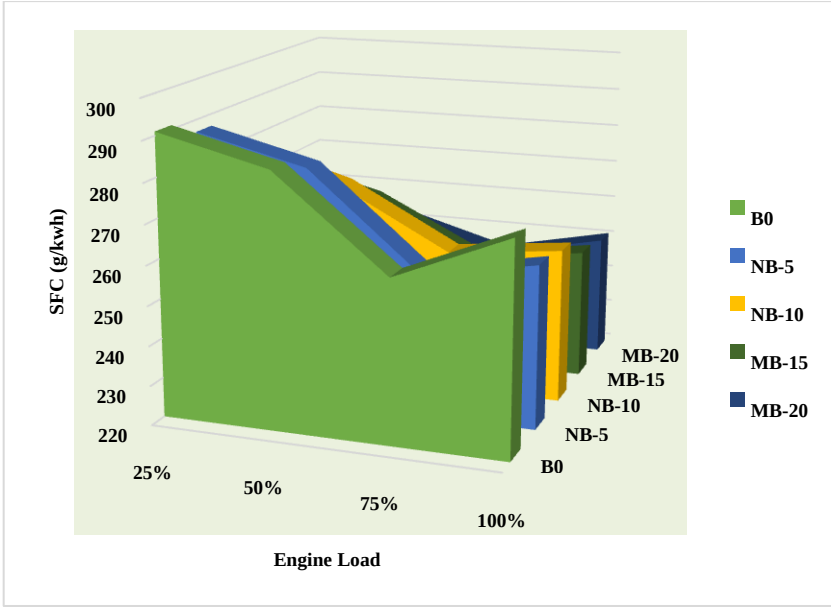

Figure 16: The relationship between engine load and BSFC for different blends.

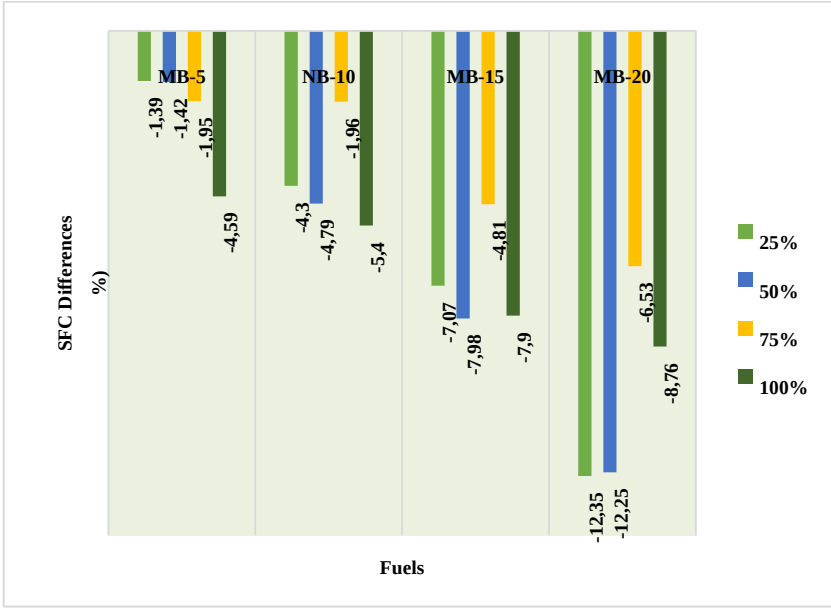

Figure 17: SFC Changeover differences.

CONCLUCSION

Mentha Tomentosa was chosen from among the essential oil plants because it has a greater oil concentration. Hydrodistillation was used to extract the essential oil first. Essential oil, its components, and fuels have several significant physical and chemical fuel qualities that have been determined. The transesterification process is used to make biodiesel from essential oils. The calorific value of menta tomentosa essential oil increased during the fuel generation process, but its viscosity and density dropped. Essential oils have a viscosity, density, and calorific value that are similar to those of reference diesel fuel when compared to other biodiesel sources.Under varied loads, mixed fuels and diesel fuel were tested for emissions and performance at 1500 constant engine rpm. The blended gasoline increased NO_x and CO_2 emissions while lowering CO and HC. Oxygenated hydrocarbons increased oxidation in the molecular structure of the essential oil, resulting in these results. Blended fuels have the following characteristics when it comes to performance: While engine power and torque increased by 8.95 percent kW and 4.28 percent Nm, specific fuel consumption dropped by 5.82 percent g/kwh. The high oxygen concentration, calorific value, and enthalpy of evaporation all contribute to these results. Consequently, essential oils can be used in diesel engines without modification. It is also a biological and environmentally friendly fuel.

REFERENCES

Akader, Y. (2006). Soya yağı metil esterinin dizel motorlarda yakıt olarak kullanımının deneysel olarak araştırılması. Yüksek Lisans Tezi, Balıkesir Üniversitesi Fen Bilimleri Enstitüsü, Balıkesir.

Al-Hasan. M. Effect of ethanol–unleaded gasoline blends on engine performance and exhaust emission. Energy Convers Manag, 44 (9) (2003), pp. 1547-1561

Amin, H. Mazaheri A review on novel processes of biodiesel production from waste cooking oil Appl Energy, 104 (2013), pp. 683-710

Başer, H. C, (1998). Tıbbi ve Aromatik Bitkilerin Endüstriyel Kullanımı, Anadolu Üniversitesi Eczacılık Fakültesi TAB Bülteni, 1998; 13-14-19-43.

Bayraktar. H. Experimental and theoretical investigation of using gasoline–ethanol blends in spark-ignition engines Renew energy, 30 (11) (2005), pp. 1733-1747

B-j. Xue, J. Luo, F. Zhang, Z. Fang (2014). Biodiesel production from soybean and Jatropha oils by magnetic CaFe 2 O 4–Ca 2 Fe 2 O 5-based catalyst Energy, 68 (2014), pp. 584-591

Canakci. M. NOx emissions of biodiesel as an alternative diesel fuel. Int. J. Veh. Des., 50 (2009), pp. 213-228

Canakci, M. Van Gerpen, J. (2001). Biodiesel production from oils and fats with high free fatty acids Transactions-American Soc Agric Eng, 44 (6) (2001), pp. 1429-1436

Celik. M.B. Experimental determination of suitable ethanol–gasoline blend rate at high compression ratio for gasoline engine Appl Therm Eng, 28 (5) (2008), pp. 396-404

Çılğın. E., (2015). 3. Nesil Biyoyakıt Teknolojisi Alglerin bir Dizel Motorunda Performans ve Egzoz Emisyonlarına Etkisinin Araştırılması. Iğdır Üni. Fen Bilimleri Enst. Der. / Iğdır Univ. J. Inst. Sci. & Tech. 5(3): 33-41, 2015

Çılğın. E.(2021). Investigation of the usability of essential oils in diesel engines as a new biodiesel source. güfbed/gustıj (2021) 11 (2): 573-585

Duren, A. Voinov, O. Arodudu, M.T. (2015). Firrisa Where to produce rapeseed biodiesel and why? Mapping European rapeseed energy efficiency Renew Energy, 74 (2015), pp. 49-59

Linskens, H. F., Jackson, J.F, 1997b Modern Methods of Plant Analysis, Vol. 12: Essential Oils and waxes, Springer, Germany

Najafi.G. B. Ghobadian, A. Moosavian, T. Yusaf, R. Mamat, M. Kettner, etal. (2016).SVM and ANFIS for prediction of performance and exhaust emissions of a SI engine with gasoline-ethanol blended fuels. Appl Therm Eng, 95 (2016), pp. 186-203

Tse. H, C.W. Leung, C.S. Cheung. Investigation on the combustion characteristics and particulate emissions from a diesel engine fueled with diesel-biodiesel-ethanol blends. Energy, 83 (2015), pp. 343-350

İlkılıç.,Çılğın.,2013. Effect Of Terebinth Oil Biodiesel On Exhaust Emissions in a Ci Engine. Batman University Journal of Life Sciences. Volume 3, Number 2 (2013)

Ilkılıc, C. and Öner, C. (2017). Bıodıesel fuel obtaıned from sunflower oıl as an alternatıve fuel for dıesel engınes. The Online Journal of Science and Technology, 7, 3.

Sarıdemir. S. Biyodizel-Dizel Yakıt Karışımlarının Motor Gürültü Ve Egzoz Emisyonlarına Olan Etkisi. Engineering and Science 3-5 November 2016 (ISITES2016 Alanya/Antalya - Turkey)

S. Pankaj, V. Tikendra Nath, P. Arivalagan. An experimental evaluation of engine performance and emission characteristics of CI engine operated with Roselle and Karanja biodiesel. Fuel, 254 (2019), Article 115652

V.A.M. Selvan, R. Anand, M. Udayakumar. Effects of cerium oxide nanoparticle addition in diesel and diesel–biodiesel–ethanol blends on the performance and emission characteristics of a CI engine J Eng Appl Sci, 4 (7) (2009), pp. 1819-6608

Viswanathan. K., ShuangWang.S. Experimental investigation on the application of preheated fish oil ethyl ester as a fuel in diesel engine. Fuel Volume 285, 1 February 2021, 119244

Yaylı, N, (2013). Uçucu Yağlar ve Tıbbi Kullanımları, Karadeniz Teknik Üniversitesi Eczacılık Fakültesi Yayınları, 2013; 1-2-4.

CHAPTER 3

CLASS-E RESONANT POWER CONVERTER DESIGN FOR WIRELESS POWER TRANSMISSION SYSTEMS

Lec. Dr. Fatih ISSI[1]

[1] Çankırı Karatekin University, Vocational School, Electronics and Automation Department, Çankırı Turkey. fatihissi@karatekin.edu.tr.ORCID ID: 0000-0001-6191-4525

INTRODUCTION

The Class-E inverter is highly suitable for use as a power inverter due to its high power conversion efficiency, low sensitivity to component changes, simple circuit topology and design techniques[1]. In Class-E inverters, the switch is operated in on-off mode, preventing high current and voltage of the switch on the load line, and shaping the output current and voltage waveform[2]. his minimizes power loss, especially during switching transitions. For this reason, Class-E inverters provide significant advantages with their single switch structure and low switching losses under constant load[3-5]. The most considerable disadvantage of Class-E inverters is that they cannot maintain constant load voltage at variable loads, and the need to regulate load variability arises[1]. Therefore, it is necessary to model the inverter mathematically and determine the parameters required for regulation. Figure 1 shows the circuit topology of the Class-E inverter.

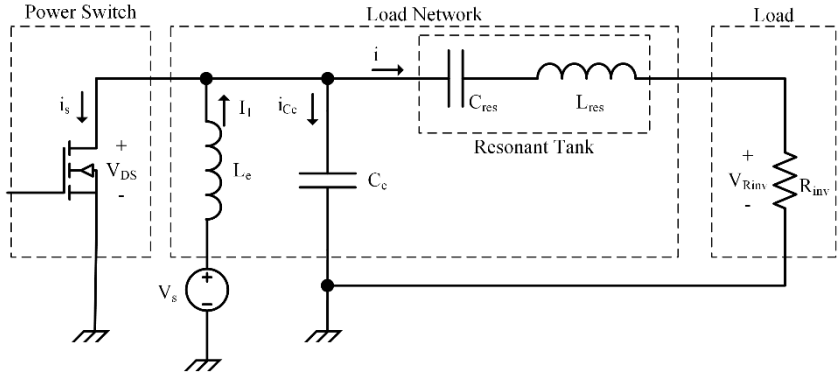

Figure 1. Class-E inverter circuit topology

In the circuit, V_S refers to the source voltage, L_e refers to the inverter input coil, S to the power switch MOSFET, C_e parallel capacitor, R_{inv} to the inverter output load, C_{res} and L_{res} resonance tank. C_e parallel capacitor and MOSFET output parasitic capacitance express the total parallel capacitance[6]. Resonant tank coil L_{res} is provided with transmitter coil, eliminating the need for additional coils. Inverter components and parameters are calculated according to the selected switching frequency and D=0.5 switching occupancy rate[7].

Zero voltage switching Class-E inverter has three different operating states and are given in Table 1[7].

Table 1. Class-E inverter operating states

State		Result
State 1	$\frac{dv_{DS}(\omega t)}{d(\omega t)} = 0$	$v_{DS}(2\pi) = 0$
State 2	$\frac{dv_{DS}d(\omega t)}{d(\omega t)} < 0$	
State 3	$\frac{dv_{DS}d(\omega t)}{d(\omega t)} > 0$	

In the three cases given in the table, when the switch is closed, the voltage falling on the switch V_{DS} and the voltage falling on the capacitor C_e becomes zero [7, 8]. With the opening of the switch, the current flowing through the choke coil flows through the capacitor C_e, forming the waveform of the switch voltage[9]. The waveforms for the three states are presented in Figure 2.

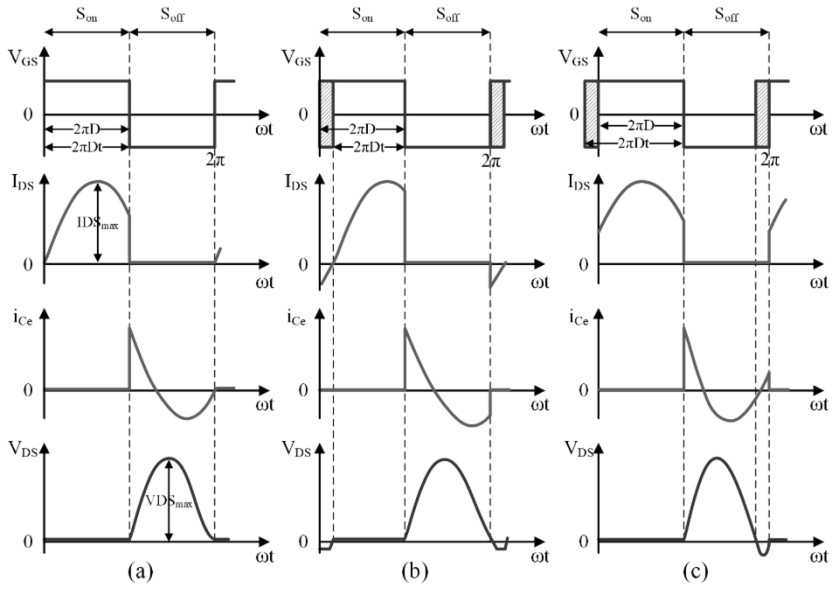

Figure 2. ZVS Class-E inverter operating states, a) state 1, b) state 2 and c) state 3

The optimum operating condition for the inverter is as given in case 1. According to Eq.1 in Case 1;

$$\frac{dv_{DS}(\omega t)}{d(\omega t)}|_{\omega t=2\pi} = 0 \qquad (1)$$

switch voltage and its derivative should be equal to zero when the switch turns on[7]. To meet this condition, the necessary component values for the inverter design are determined depending on the load resistance. Optimum operation is only possible at optimum load resistance value[9]. When the load resistance is higher than the optimum load resistance, the peak value of the current through the resonant circuit will be lower than the current required for optimum operation. In case 2, the voltage falling on the capacitor C_e decreases,

and the switch voltage becomes higher than zero at the moment of switching. Conversely, in case 3, when the load resistance value is lower than the optimum load resistance, the peak value of the current flowing through the resonant circuit will be higher than the current required for optimum operation. In this case, the voltage falling on the capacitor C_e increases, and the switch voltage becomes less than zero [7].

In the design phase, the analysis of the waveforms of the inverter current and voltage given in Figure 2 is based on the sinusoidal current from the series resonant circuit[7]. The expression of the current passing through the series resonance circuit is as given in Eq.2.

$$i = I_m \sin(\omega t + \varphi) \tag{2}$$

In the equation, Im represents the amplitude of the current and φ represents the initial phase angle. The sum of the current (i_s) through the switch and the current of the capacitor C_e is equal to the difference between the current drawn from the source and the resonant circuit currents, as given in Eq.

$$i_s + i_{Ce} = I_1 - I_m \sin(\omega t + \varphi) \tag{3}$$

For switching time interval $0<wt\leq 2\pi D$, the switch is conducting and the current through capacitor C_e becomes $i_{ce}=0$. According to Eq.4, the current passing through the switch is calculated as.;

$$i_s = \begin{cases} I_1 - I_m \sin(\omega t + \varphi), & 0 < \omega t \leq 2\pi D \\ 0 \quad , & 2\pi D < \omega t \leq 2\pi \end{cases} \tag{4}$$

For the switching time interval $2\pi D<\omega t\leq 2\pi$, the switch is cutoff and the current through the switch $i_s=0$. According to Eq.5, the current passing through the capacitor C_e is;

$$i_{Ce} = \begin{cases} 0 & , \ 0 < \omega t \leq 2\pi D \\ I_1 - I_m \sin(\omega t + \varphi), & 2\pi D < \omega t \leq 2\pi \end{cases} \quad (5)$$

The voltage falling on the switch and the capacitor C_e becomes $v_s=0$ when the switch is conduction. When the switch is in cutoff, it is calculated as given in Eq.6, depending on the voltage of the C_e capacitor.

$$v_s = \frac{1}{\omega C_e} \int_{2\pi D}^{\omega t} i_{Ce} d(\omega t) \quad (6)$$

Solution of the equation according to time intervals as expressed in Eq.7;

$$v_s = \begin{cases} 0 & , \ 0<\omega t\leq 2\pi D \\ \frac{1}{\omega C_e}+(I_{in}(\omega t-2\pi D)+ & , \ 2\pi D<\omega t\leq 2\pi \\ I_m \cos(\omega t+\varphi)-\cos(2\pi D+\varphi) & \end{cases} \quad (7)$$

Out of the range where the switch voltage is zero, the relationship between the input current I_1, the switching occupancy rate D and the phase angle φ is Eq.8 is expressed as;

$$I_m = I_1 \frac{2\pi(1-D)}{\cos(2\pi D+\varphi)-cos\varphi} \quad (8)$$

When the amplitude of the current passing through the resonant circuit is substituted in the switch voltage equation, the switch voltage shown in Eq.9 is obtained.

$$v_s = \begin{cases} 0 & ,0 < \omega t \leq 2\pi D \\ \left\{ \frac{\omega t - 2\pi D + \frac{2\pi(1-D)[\cos(\omega t+\varphi)-\cos(2\pi D+\varphi)]}{\cos(2\pi D+\varphi)-cos\varphi}} \right\} & ,2\pi D < \omega t \leq 2\pi \end{cases} \quad (9)$$

For case 1 given in Table 1, the relationship between phase angle φ and switching occupancy ratio D is according to Eq.10 is expressed as.;

$$tan\varphi = \frac{\cos 2\pi D - 1}{2\pi(1-D)+sin2\pi D} \quad (10)$$

The phase angle is obtained by using Eq.11.

$$\varphi = \pi + arctan\left[\frac{\cos 2\pi D - 1}{2\pi(1-D)+sin2\pi D}\right] \quad (11)$$

The source voltage V_s can be calculated as given in Eq.12.

$$V_s = \frac{1}{2\pi}\int_{2\pi D}^{2\pi} v_s d(\omega t) \quad (12)$$

Substitute the switch voltage expression in the equation Eq.13;

$$V_s = \frac{I_1}{\omega C_e}\left\{\frac{(1-D)[\pi(1-D)cos\pi D+sin\pi D]}{\tan(\pi D+\varphi)sin\pi D}\right\} \quad (13)$$

is obtained. From here, the inverter input resistance can be easily found as expressed in Eq.14.

$$R_i = \frac{V_s}{I_1} = \frac{(1-D)[\pi(1-D)cos\pi D+sin\pi D]}{\omega C_e \tan(\pi D+\varphi)sin\pi D} \quad (14)$$

In the inverter, the ZVS condition is satisfied in the range of $0 \leq R_{inv} < R_{opt}$ for optimum load resistance R_{opt}, but not in the case of $R_{inv} > R_{opt}$ [5]. The input voltage according to Eq.15 for the switching ratio D=0.5 available as.;

$$V_s = \sqrt{\frac{R_{inv}(\pi^2+4)P_o}{8}} \quad (15)$$

According to Eq.16, the input resistance of the inverter is calculated as;

$$R_i = \frac{(\pi^2+4)}{8} R_{inv} \quad (16)$$

When the obtained input resistance and the output equivalent resistance are equal, the maximum power transfer for the inverter is realized[12, 13]. The maximum value of the output voltage in the expression given in Eq.17;

$$V_{MR_{inv}} = \frac{4}{\sqrt{(\pi^2+4)}} V_s \quad (17)$$

It is calculated based on the input voltage. One of the limiting variables in Class-E inverters is the maximum value of the voltage falling on the power switch[2] and;

$$V_{SM} = 3.562 V_s \quad (18)$$

is obtained as. The total current drawn from the source is expressed as in Eq.19, depending on the input voltage and load resistance.

$$I_1 = \frac{8}{\pi^2+4} \frac{V_s}{R_{inv}} \quad (19)$$

Also, the current drawn from the source determines the maximum value of the current flowing through the power switch. It constitutes another most critical parameter in power switch selection[2]. The maximum value of the current passing through the power switch is calculated as given in Eq.20.

$$I_{SM} = \left(\frac{\sqrt{(\pi^2+4)}}{2} + 1\right) I_1 \quad (20)$$

In addition, the amplitude of the current passing through the resonance tank is given in Eq.21;

$$I_m = I_1 \frac{\sqrt{(\pi^2+4)}}{2} \quad (21)$$

The components calculated in the inverter design determine the switch voltage. The waveform of the voltage falling on the switch (V_{DS}) shows whether the load match is achieved or not[2]. The waveform of the load-matched switch voltage is presented in Figure 3.

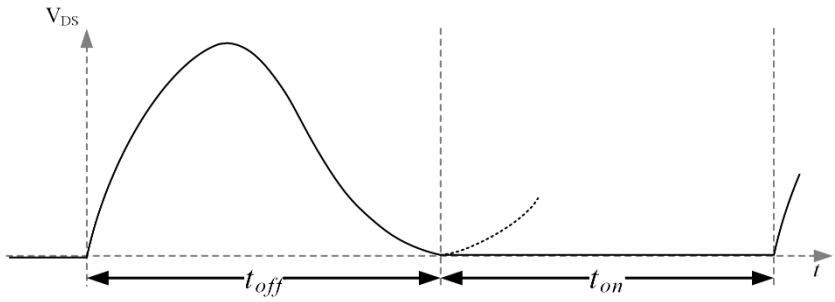

Figure 3. Switch voltage (V_{DS}) waveform when load matched

In cases where load compatibility cannot be achieved, the values of the circuit components must be changed. The changes that will occur in the switch voltage while adjusting the parameters are given in Figure 4.

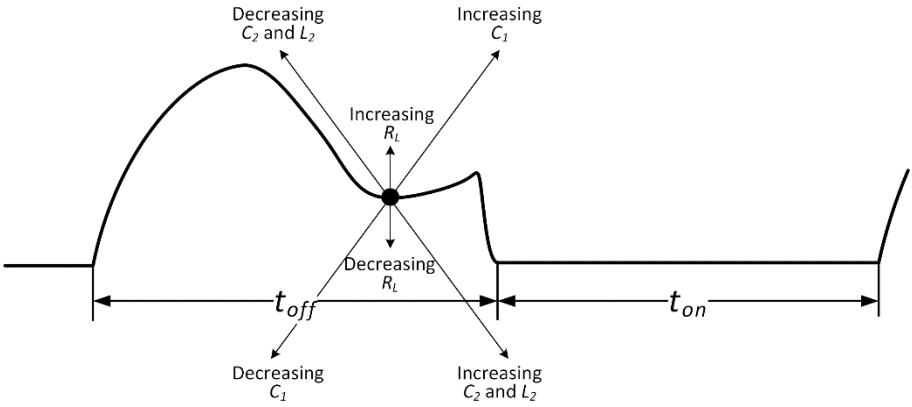

Figure 4. Effect of circuit components on switch voltage waveform

As can be seen in the graph, increasing the value of the C_e capacitor moves the groove formed in the switch voltage up and to the right. Increasing the value of the C_{res} capacitor moves the trough down and to the right. Increasing the L_{res} value again moves the trough down and to the right. Increasing the load resistance moves the trough upwards and decreasing it moves it downwards [2]. The values of the circuit components are adjusted in this way until the waveform given in Figure 3 is obtained. Adjustment is complete when the waveform is as shown in Figure 3. However, to change the parameters, changes must be made in the circuit components. It is observed that changing the capacitance values by determining the coil and load resistance is a frequently used method when the studies in the literature are examined[14-16]. In the tuning process, the load resistance is approximated first. The L_{res} value is adjusted depending on the Q_L quality factor[17]. The quality factor should be taken as at least 2.5[2,

18]. A hard switching situation occurs at a lower quality factor value[18]. The system's operating frequency is determined, and the occupancy is set as 50% [2, 18, 19]. After these operations, the critical waveform given in Figure 3 is observed. The waveform in Figure 3 is obtained by adjusting the C_e and C_{res} capacitances according to the situations presented in Figure 4. Then, if the V_s source voltage is at the desired value, the load compatibility is achieved. If V_s is not at the desired value, it is adjusted and the previous step is repeated. The voltage V_s changes the switch capacitance value, so the capacitance C_e changes[2]. The waveform of the V_{DS} voltage in the case of the inverter load matching is exemplified in Figure 5(a), and the waveform of the case where the load matching is not achieved is illustrated in the Figure 5(b).

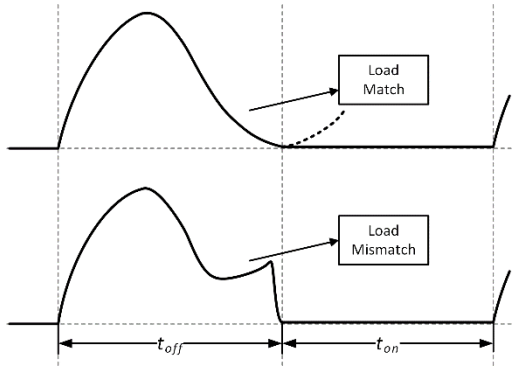

Figure 5. Switch voltage (V_{DS}) waveform with and without load matching

1. INVERTER COMPONENTS

In Class-E inverters, the load resistance value is in the design center[1]. The output power of the inverter varies inversely with the load resistance and is directly proportional to the square of the input voltage[20]. Accordingly, there are two ways to increase the output power. These are to reduce the load resistance or increase the input voltage. Reducing the load resistance is possible with impedance conversion[21, 22]. A high impedance conversion ratio increases the cost and power loss[20]. Reducing the input voltage is more efficient as it affects quadratic. In Class-E inverters, the drain voltage is 3.56 times the source voltage, creating a break-down hazard on the switch[23].

When the switch is closed since C_e and C_{oss} will be short-circuited, the fr1 frequency given in Eq.22 appears, and when the switch is opened, C_e and C_{oss} will form an equivalent (C_{eq}) in parallel, so the f_{r2} frequency given in Eq.23 appears[8].

$$f_{r1} = \frac{1}{2\pi\sqrt{L_{res}C_{res}}} \tag{22}$$

$$f_{r2} = \frac{1}{2\pi\sqrt{L_{res}C_{eq}}} \tag{23}$$

For ZVS condition, f_{r1} must be lower than switching frequency and switching frequency must be lower than f_{r2}. Another requirement is that the half-period sums of f_{r1} and f_{r2} should be close to the switching frequency (f_{sw}) and slightly higher. The resonant circuit will behave inductively when the switching frequency f_{sw} is higher than f_{r1} [7].

Therefore, the L_{res} inductance will be divided into two inductances, forming the series-connected inductances L_{resa} and L_{resb}. The L_{resa} and C_{res} capacitor will resonate at the switching frequency fsw.

$$\omega = \frac{1}{\sqrt{L_{resa}C_{res}}} \tag{24}$$

The loaded quality factor of the system can be calculated as given in Eq.25.

$$Q_L = \frac{\omega L_{res}}{R_{inv}} = \frac{1}{\omega C_{res} R_{inv}} + \frac{\omega L_{resb}}{R_{inv}} \tag{25}$$

The load resistance changes depending on the output power of the inverter, as seen in Eq.26.

$$R_{inv} = \frac{(8V_s^2)}{(\pi^2+4)P_{Linv}} \tag{26}$$

Here, the input voltage V_s required for a constant load resistance and constant power can be calculated. In this way, the needed V_s value for the initial condition is obtained. The variable load resistor must change the input voltage as seen in the equation. Otherwise, the output power will change.

The required L_{res} and C_{res} values for the resonance tank to be used at the inverter output are calculated according to Eq.27 and Eq.28, depending on the quality factor. When the C_{res} resonance capacitor is combined with the WPT system, it will be expressed as the C_1 capacity, which includes both the inverter resonance capacity and the resonance capacity of the WPT system. The quality factor must be high enough (Q_L>1.7879) for the output current to be sinusoidal[2].

$$C_{res} = \frac{1}{\omega Q_L R_{inv}}$$

(27)

$$L_{res} = \frac{Q_L R_{inv}}{\omega} \quad (28)$$

The resonance condition changes depending on the frequency and is calculated for a fixed frequency. In addition, the L_{res}, C_{res} and C_e value directly affect the waveform of the switch voltage in Figure 3 for the realization of ZVS.

The capacity of the resonance tank and the amplitude of the voltage falling on its coil are as given in Eq.29 and Eq.30;

$$V_{Cm} = \frac{I_m}{\omega C_{res}} \quad (29)$$

$$V_{Lm} = \omega L_{res} I_m \quad (30)$$

The power consumed in the resonance tank is Eq.31 and Eq.32;

$$P_{rLres} = \frac{r_L {I_m}^2}{2} \quad (31)$$

$$P_{rCres} = \frac{r_C {I_m}^2}{2} \quad (32)$$

Power switch parallel capacitance value C_e is calculated according to the selected load resistance as expressed in Eq.33. Also, since this capacitance is connected in parallel to the MOSFET, the output parasitic capacitance value C_{oss} should be added to this value[2].

$$C_e = \frac{8}{\pi(\pi^2+4)\omega R_{inv}} \quad (33)$$

The DC bus coil L_e located at the input of the inverter is there to provide constant current and should be large enough[18]. This current, which will be transmitted to ground when the switch is open, is shared between C_{oss}, C_e and L_{res} when the switch is closed. According to Eq.34, the lowest L_e value that can be used is;

$$Le_{min} = \frac{(\pi^2+4)R_{inv}}{f_{sw}} \quad (34)$$

The power dissipated in the input coil is calculated according to Eq. 35 using the coil internal resistance r_{Le} and the input current I_1.

$$P_{rLe} = r_{Le}{I_1}^2 \quad (35)$$

Using the RMS value of the current passing through the power switch Eq.36;

$$I_{Srms} = \frac{I_1\sqrt{(\pi^2+28)}}{4} \quad (36)$$

is calculated and used to find the switch power consumption as in Eq.37.

$$P_{rDS} = r_{DS}{I_{Srms}}^2 \quad (37)$$

The current passing through the parallel capacity is;

$$I_{Cerms} = \frac{I_1\sqrt{(\pi^2-4)}}{4} \quad (38)$$

calculated using and the power consumed on the capacity is according to Eq.39;

$$P_{rCe} = r_{Ce}{I_{Cerms}}^2 \quad (39)$$

With the total power values consumed in the components;

$$P_r = P_{rLe} + P_{rDS} + P_{rCe} + P_{rL} + P_{rC} \quad (40)$$

The ratio of the total power loss P_r to the output power P_o creates the inverter efficiency ηinv given in Eq.41.

$$\eta_{inv} = \frac{P_o}{P_o + P_r} \quad (41)$$

2. Inverter Impedance Analysis

The impedance analysis of the serial-to-serial wireless energy transmission system with the Class-E inverter is necessary for tuning the capacitance array. Therefore, the inverter impedance analysis is considered in conjunction with the WPT system. The circuit topology of the combined inverter and WPT system is given in Figure 6.

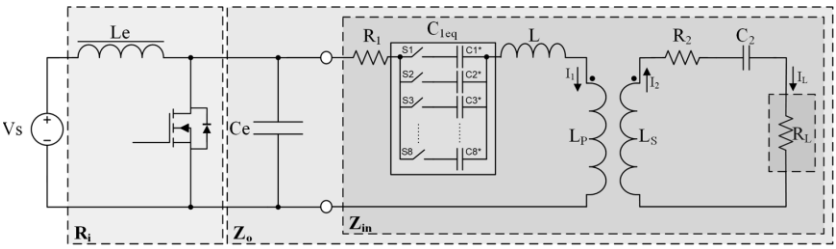

Figure 6. Integrated Class-E inverter and circuit topology of WPT system

In the WPT system given in the figure, the equivalent load impedance of the inverter consists of the inverter output load Z_{in}, the self-inductance of the L_P emitter coil, the resistance of the emitter coil R_1, the self-inductance of the L_S receiver coil, the resistance of the R_2 receiver coil, and the resonance capacity of the receiver circuit C_2.

The back-inverter output load can be arranged to include the mutual inductance M and the receiver part impedance Z_2 given in Figure 7

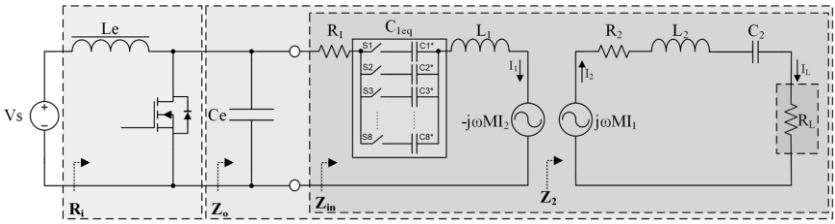

Figure 7. Presentetaion of mutual inductance on the circuit topology of the integrated Class-E inverter and WPT system

Here, the receiver circuit equivalent impedance Z_2 is given in Eq.42, and the receiver circuit resonance capacitance C_2 and the load resistor R_L represent the load impedance Z_L.

$$Z_2 = j\omega L_2 + \frac{1}{j\omega C_2} + R_L \tag{42}$$

The output load of the system can be simplified as given in Figure 8. Here is the reflected impedance Z_r, which will represent the inverter load.

The reflected impedance Z_r is formed by the effect of the receiver circuit on the emitter circuit and varies depending on the coupling coefficient k between the transmitter-receiver coils. Capacitor C_2 in the receiver circuit is present and fixed to eliminate the leakage inductance of the receiver coil and ensure that the receiver circuit operates in resonance. The mutual inductance M between the transmitter and receiver coils is expressed in coil inductances, as seen in Eq.43 and the coupling coefficient k [24].

$$L_1 = L_{lp} + M \tag{43}$$

$$M = k\sqrt{L_1 L_2} \tag{44}$$

The inductance L_1 given in Eq.44 consists of the sum of the leakage inductance L_{lp} of the emitter coil and the mutual inductance M. The reflected impedance forming the inverter output load is expressed as given in Eq.45.

$$Z_r = \frac{\omega^2 M^2}{R_2 + Z_2} \tag{45}$$

If R_2 is neglected because the receiver coil resistance is much lower than Z_2, the real component of the reflected impedance can be written as Eq.46, and the imaginary component can be written as Eq.47[25].

$$ReZ_r = \frac{\omega^4 C_2^2 M^2 R_L}{(\omega^2 C_2 L_2 - 1)^2 + \omega^2 C_2^2 R_L^2} \tag{46}$$

$$ImZ_r = \frac{-\omega^3 C_2 M^2 (\omega^2 C_2 L_2 - 1)}{(\omega^2 C_2 L_2 - 1)^2 + \omega^2 C_2^2 R_L^2} \tag{47}$$

When the system operates at the resonant frequency, Eq.46 and Eq.47 are simplified as seen in Eq.48 and Eq.49, since $\omega = 1/\sqrt{L_2 C_2}$.

$$ReZ_r = \frac{\omega^2 M^2}{R_L} \tag{48}$$

$$ImZ_r = 0 \tag{49}$$

When the inverter output resonance condition is fulfilled, $j\omega L_1 + \frac{1}{j\omega C_1} = 0$ becomes =0 [26]. In this case, the input impedance of the WPT system Z_{in} is expressed as in Eq.50.

$$Z_{in} = R_1 + \frac{j\omega M^2}{Z_r} \quad (50)$$

Serial-Serial topology has two main advantages when applied in fixed distance range and fixed capacity. First, the reflected impedance of the receiver circuit to the transmitting circuit has only a real component, and the imaginary component is zero. When the receiving circuit is operated at the resonant frequency, it only consists of the active component. Second, the transmit and receive circuit capacities are load independent. In this case, the capacitance values depend only on the transmit-receive winding inductances[27]. In the case of variable distance, the mutual inductance M changes the reflected impedance Z_r.

The control of the WPT system input impedance Z_{in} and the load matching of the Class-E inverter simultaneously can be done depending on the change of the transmit coil input impedance Z_{TX}. Transmitter coil input impedance is Eq.51.;

$$Z_{TX} = R_{TX} + j\omega X_{TX} \quad (51)$$

The real component R_{TX} given in Eq.52 can be written depending on the coupling coefficient.

$$R_{TX} = \frac{\omega^4 C_2^2 R_L L_p^2 [(1-k)+2k+1]}{(1-\omega^2 C_2 L_p)^2 + (\omega R_L C_2)^2} \quad (52)$$

The transmitter coil inductance L_p takes the value $Lp = (L_0 + k/(L_0 + 1))$ because it contains the resonance inductance. When capacitor C_2, RL load resistance, and operating frequency are kept constant, the real component of the emitter coil input impedance

changes depending on the R_{TX} coupling coefficient. If the imaginary component given in Eq.53 is expressed as;

$$X_{TX} = \frac{\omega L_p(\omega^2 C_2^2(1-k)L_p^3+1-\omega^2 L_p^2 C_2-\omega^2 C_2(1-k)L_p+\omega^2 R_L^2 C_2^2)}{(1-\omega^2 C_2 L_p)^2+(\omega R_L C_2)^2} \quad (53)$$

and the coupling coefficient varies depending on k. The obtained transmitter coil input resistance R_{TX} is directly related to the load resistance RL and is used to determine the regions where the ZVS condition will be valid. In this way, the coil input resistance R_{TX}, which changes depending on the distance, can be controlled by the capacitance array.

The equivalent impedance Z_o seen at the inverter output consists of the emitter coil input impedance Z_{TX} and the parallel capacitor C_e. As seen in Eq.54, the output impedance is not found in Z_o under the conditions that C_{1eq} and L_{res} components meet the resonance condition.

$$Z_o = \frac{R_{TX}+j\omega(L_0+M)\left(1-\omega^2(L_0+M)C_e-\frac{C_e R_{TX}^2}{(L_0+M)}\right)}{(1-\omega^2(L_0+M)C_e)^2+(\omega C_e R_{TX})^2} \quad (54)$$

According to the phase angle of the inverter resonance circuit ϕopt Eq.55, to realize the optimum operating conditions of the inverter, ZVS and ZDS should be[28];

$$\phi_{opt} = tan^{-1}\left(\frac{2}{\pi}\right) = 32{,}48° \quad (55)$$

The equivalent phase angle ϕ_{eq} of the inverter is found as given in Eq.56[7].

$$\phi_{eq} = tan^{-1}\left[\frac{\omega(L_0+M)\left(1-\omega^2(L_0+M)C_e-\frac{C_e R_{TX}^2}{(L_0+M)}\right)}{R_{TX}}\right] \quad (56)$$

When the ϕ_{opt}= ϕ_{eq} condition is met, the inverter is at the optimum operating point, and ZVS and ZDS are realized.

By calculating the transmitter coil input resistance, R_{TX}, which includes the emitter coil impedance and the reflected impedance, the impedance formed by the components other than the capacitance array at the inverter output is thus calculated.

CONCLUSIONS

Class-E inverter with low power loss, which can be used in wireless energy transmission systems, has been analyzed. The calculation of the components required for the design of the inverter is given in detail. In addition, the reflection of the input impedance of the WPT system to the Inverter is discussed. Equivalent impedance analysis that will cause a load change at the inverter output has been made.

REFERENCES

1. Zulinski R. A high-efficiency self-regulated class E power inverter/converter. IEEE transactions on industrial electronics. 1986, 33, 340-2.
2. Sokal NO. Class-E RF Power Amplifiers. 2001.
3. Raab F. Idealized operation of the class E tuned power amplifier. IEEE Transactions on Circuits and Systems. 1977, 24, 725-35.
4. Lotfi A, Medi A, Katsuki A, Kurokawa F, Sekiya H, Kazimierczuk MK, et al. Subnominal Operation of Class-E Nonlinear Shunt Capacitance Power Amplifier at Any Duty Ratio and Grading Coefficient. IEEE Transactions on Industrial Electronics. 2018, 65, 7878-87.
5. Kazimierczuk MK. RF Power Amplifiers. Wiley2008.
6. Ayachit A, Corti F, Reatti A, Kazimierczuk MK. Zero-Voltage Switching Operation of Transformer Class-E Inverter at Any Coupling Coefficient. IEEE Transactions on Industrial Electronics. 2019, 66, 1809-19.
7. Marian K. Kazimierczuk DC. Resonant Power Converters. 2nd ed. Wiley2011.
8. Green PB. Class-E power amplifier design for wireless power transfer. Infineon. 2018.
9. Kazimierczuk M, Puczko K. Exact analysis of class E tuned power amplifier at any Q and switch duty cycle. IEEE Transactions on Circuits and Systems. 1987, 34, 149-59.
10. Chen YF, Zhang HL, Park SJ, Kim DH. A Switching Hybrid LCC-S Compensation Topology for Constant Current/Voltage EV Wireless Charging. Ieee Access. 2019, 7, 133924-35.
11. Wireless Power Transfer for Light-Duty Plug-in/Electric Vehicles and Alignment Methodology. SAE International2020.
12. Wei X, Wang Z, Dai H. A Critical Review of Wireless Power Transfer via Strongly Coupled Magnetic Resonances. Energies. 2014, 7, 4316-41.
13. Mai R, Ma L, Liu Y, Yue P, Cao G, He Z. A Maximum Efficiency Point Tracking Control Scheme Based on Different Cross Coupling of Dual-Receiver Inductive Power Transfer System. Energies. 2017, 10.

14. Huang ZH, Wang L, Zhang YX, Liu RT. Design of WPT RF Power Supply Based on Dual Directional Coupler and Capacitor Array Impedance Matching Network. Ieee Access. 2020, 8, 68209-18.
15. Lim Y, Tang H, Lim S, Park J. An Adaptive Impedance-Matching Network Based on a Novel Capacitor Matrix for Wireless Power Transfer. IEEE Transactions on Power Electronics. 2014, 29, 4403-13.
16. Waters B, Sample A, Smith J. Adaptive impedance matching for magnetically coupled resonators. PIERS Proceedings. 2012, 694-701.
17. Timilsina A, Nepali B, Paudyal B, Kunwar JD. Design and Performance Analysis of Highly Efficient Class E Resonant Inverter. Zerone Scholar. 2016, 1, 14-7.
18. Class-E power amplifier design for wireless power transfer. 2018.
19. Ponte J, Ghahremani A, Huiskamp M, Annema A, Nauta B. Theory and Implementation of a Load-Mismatch Protective Class-E PA System. IEEE Transactions on Circuits and Systems I: Regular Papers. 2020, 67, 369-77.
20. Du J-C, Wang Z-G, Xu J, Yang Y-F. A Current-Injection Class-E Power Amplifier. IEEE Microwave and Wireless Components Letters. 2020, 30, 775-8.
21. Park C, Kim Y, Kim H, Hong S. A 1.9-GHz CMOS Power Amplifier Using Three-Port Asymmetric Transmission Line Transformer for a Polar Transmitter. IEEE Transactions on Microwave Theory and Techniques. 2007, 55, 230-8.
22. Lee O, An KH, Kim H, Lee DH, Han J, Yang KS, et al. Analysis and Design of Fully Integrated High-Power Parallel-Circuit Class-E CMOS Power Amplifiers. IEEE Transactions on Circuits and Systems I: Regular Papers. 2010, 57, 725-34.
23. Sokal NO, Sokal AD. Class E-A new class of high-efficiency tuned single-ended switching power amplifiers. IEEE Journal of Solid-State Circuits. 1975, 10, 168-76.

24. Moon S, Kim B, Cho S, Moon G. Analysis and design of wireless power transfer system with an intermediate coil for high efficiency. 2013 IEEE ECCE Asia Downunder, Melbourne, Australia, 2013. p. 1034-40.
25. Xun L, Ng WM, Lee CK, Hui SY. Optimal operation of contactless transformers with resonance in secondary circuits. 2008 Twenty-Third Annual IEEE Applied Power Electronics Conference and Exposition, Austin, Texas, 2008. p. 645-50.
26. Fu M, Zhang T, Zhu X, Ma C. A 13.56 MHz wireless power transfer system without impedance matching networks. 2013 IEEE Wireless Power Transfer (WPT), Perugia, Italy, 2013. p. 222-5.
27. Chopra S, Bauer P. Analysis and design considerations for a contactless power transfer system. 2011 IEEE 33rd International Telecommunications Energy Conference (INTELEC), Amsterdam, Netherlands, 2011. p. 1-6.
28. Suetsugu T, Kazimierczuk MK. Design procedure of class-E amplifier for off-nominal operation at 50% duty ratio. IEEE Transactions on Circuits and Systems I: Regular Papers. 2006, 53, 1468-76.

CHAPTER 4

MAGNETIC RESONANCE COUPLED WIRELESS POWER TRANSMISSION SYSTEMS FOR ELECTRIC VEHICLES

Lec. Dr. Fatih ISSI[1]

[1] Çankırı Karatekin University, Vocational School, Electronics and Automation Department, Çankırı Turkey. fatihissi@karatekin.edu.tr.ORCID ID: 0000-0001-6191-4525

INTRODUCTION

There are two types of charging systems in electric vehicles, wired and wireless [1]. A wired charging system charges the energy in the charging stations by connecting them to the vehicle's charging port through a cable [1]. On the other hand, a wireless charging system transfers energy to the vehicle using various energy transfer methods without using cables or physical connections[1-13]. There are different charging units used for wired charging of electric vehicles. The structure of the vehicle's charging system determines the type of charging station[3]. The main difference is whether the energy type of the charging unit is alternating current (AA) or direct current (DC). Some standards are prepared in different countries and continents, and charging units are available regionally [14]. While AA charging units must have an internal charging unit on the vehicle, it is unnecessary to have a charge control unit in DC charging stations. While any socket can be used in AC charging systems, reaching the charging station for DC charging is mandatory. Environmental disadvantages prevail in both systems [14]. Wireless Power Transmission (WPT) systems can be examined in 3 classes listed below according to their working structure [15, 16].

- Electromagnetic radiation
- Electric field coupling
- Magnetic field coupling

Electromagnetic radiation; is based on converting electrical energy into electromagnetic energy (such as microwave, a laser beam) and

converting it back into electrical energy with a silicon rectifier antenna [15, 17, 18]. It is suitable for long-distance power transmission in aerospace and military applications due to its high power density and good steering properties. However, it is not suitable for daily use [19].

Electric field coupling covers the distribution of the surface charge of the objects[6, 9, 13, 17, 18, 20-31]. It works with the resonant transmitter and the resonant receiver coupling, which creates an alternating electric field with a high frequency and high voltage source. Transmission efficiency may be affected by surrounding objects [24, 32]. The transmission power is relatively low. Magnetic Resonance coupling can be classified as short-range electromagnetic induction and mid-range strong coupling magnetic resonance when looking at the transmission distance[33]. Transmission efficiency and power are generally high in electromagnetic induction. Nevertheless, the transmission distance is limited to the centimeter level. The magnetic resonance coupled wireless power transmission (MRCWPT) system, on the other hand, has slightly less transmission efficiency and power. However, the transfer distance can reach the meter level, which is called mid-range [19]. In close-range wireless charging systems, the DC source is converted to an AC source via an inverter. Switched inverters such as H-Bridge, D-Class, and E-Class are preferred [34, 35]. The alternating voltage obtained at the inverter output is applied to the transmitter coil. The magnetic field lines formed around the transmitter coil cut the receiver coil and induce a voltage in the receiver part. The induced alternating voltage is transferred to the device to be charged or powered by the rectifier [16,

32, 36]. The basic principle of the MRCWPT system is based on the efficient transfer of energy by two resonators with the same resonance frequency[37]. In this method, the alternating voltage produced by a high-frequency inverter transfers energy by resonating the transmitter and receiver circuit[33]. By matching the transmitter part's inductance and the receiver part's inductance, a voltage should be applied at a frequency at which the circuit will resonate at the same impedance [33]. This method is most suitable for the vehicle height distance required for charging electric vehicles [36]. The block diagram of the magnetic resonance coupling is shown in Figure 1.

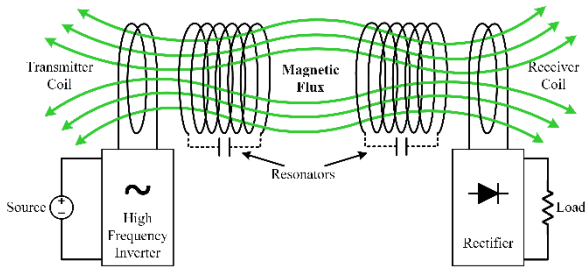

Figure 1. MRCWPT block diagram

Two types of resonant coils are used in the MRCWPT system. These are a self-resonator coil with inductance and inter-winding parasitic capacitance, and a resonator coil with an external capacitance added [38]. Coils that are resonators have the advantage of low loss, but their application is complex at low frequencies because the capacitance between turns is very low. MRCWPT systems are used in many applications such as charging electric vehicles, consumer electronics,

intelligent mobile devices, biomedical applications, robots [6, 17, 18, 24, 34, 39, 40]. With the MRCWPT system, wireless power transfer can be done in the broader area and higher efficiency[17]. The efficiency can also be high when the receiver and transmitter coils are removed [41, 42]. Since the materials in the environment do not match the resonance frequency, they do not interact with the magnetic field. Therefore, operating in the high-frequency band is another advantage for the environment and human safety. It is very efficient in mid-range applications[37]. In the MRK system, the power transfer can reach the meter level, called the middle distance. Therefore, MRCWPT is the most suitable transfer method for electric vehicles' ground clearance[20, 21]. Being multi-axis directional also makes it advantageous[37]. These advantages help to improve the performance of the wireless power transmission system in various power transmission applications[37]. The disadvantage of the MRCWPT system is that it requires a more extensive area due to its structure [6].

1. MRCWPT Circuit Topologies

For the wireless charging of the electric vehicle, a fixed transmitting coil and a vehicle-fixed receiver coil must be designed. There are four different circuit topologies to enable the MRCWPT system to resonate. These topologies are shown in Figure 2.

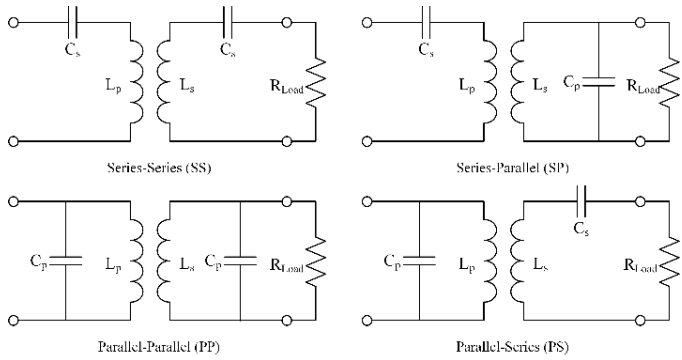

Figure 2. Basic MRCWPT Resonance Topologies

All of these topologies have advantages and disadvantages. According to the results obtained in comparative studies in wireless charging of electric vehicles, Series-Series (SS) resonance topology was more advantageous[43-46]. In high-power applications using Series-Series resonance topology, losses are considerably reduced if an LC filter is at the source output[43]. The comparison of the topologies is given in Table 1.

Table 1: MRCWPT Resonance topologies according to advantages and disadvantages

	SS	SP	PS	PP
Transmission Power	+++++	++++	+	++
Transmission Distance	++++	+	+	+
Transfer Efficiency	+++++	+	++++	++++
Load Value	↕	↔	↕	↔
Alignment Precision	+	+	++++	+++++

+: Very low, ++: Low, +++: Medium, ++++: High, +++++: Very high, ↕: Variable, ↔: Constant

1.1. Series-Series MRCWPT System

The equivalent circuit model of the MRCWPT system with a serial-to-serial topology is shown in Figure 3.

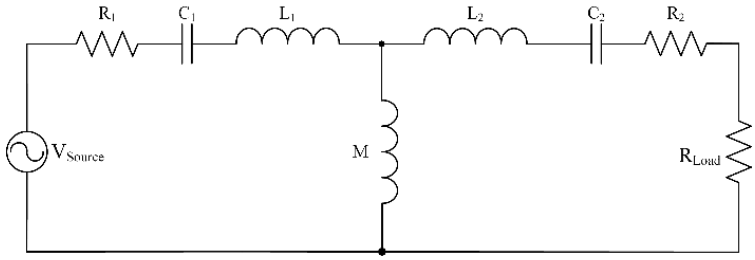

Figure 3. Series-Series MRCWPT equivalent circuit

The equivalent impedance value of the circuit is expressed as in Eq.1.

$$Z = R_1 + j\omega(L_1 - M) + \frac{1}{j\omega C_1} + \left(\frac{j\omega M(R_2+R_{Load}+j\omega(L_2-M)+\frac{1}{j\omega C_2})}{R_2+R_{Load}+j\omega L_2+\frac{1}{j\omega C_2}+M}\right) \quad (1)$$

Considering the equivalent circuit equation, the resistance of the emitter coil is expressed as R_1, and L1 expresses its self-inductance. The resonance condition of the emitting part is provided by using a series capacitor C_1. Likewise, the resistance of the receiver coil is expressed by R_2, and L2 expresses its self-inductance. For the receiver part to resonate, a series capacitor C_2 is used. The mutual inductance value, which is the effect of the two coils on each other, is expressed with M.

If the constant terms in the MRCWPT system are considered the inductance values of the coils, the resistance values, and the source frequency, the equivalent impedance of the system becomes dependent on the mutual inductance and capacitor values. The mutual

inductance value of the coils is inversely proportional to the distance change between the coils and cannot be controlled. For the efficiency to be at the highest level in the MRCWPT system, the equivalent impedance value of the system must be equal to the source impedance and load impedance. Considering that the impedance is equal in wireless charging applications in electric vehicles, the vehicle's height directly affects the mutual inductance value. It changes the equivalent impedance value of the system. Increasing or decreasing the equivalent impedance can negatively affect the efficiency of the WPT system. To eliminate this negative effect of mutual inductance, it becomes necessary to readjust the capacitor values in the system.

2. MRCWPT System Design

2.1. Analysis of Coil Inductances

In MRCWPT systems, the transmitter and receiver coils are designed as air cores. According to Ampere's law, a magnetic field is formed around a current-carrying wire. This magnetic field and the current that creates it are linearly proportional. According to Faraday's law, it is seen that a variable magnetic field induces a voltage, and this voltage is directly proportional to the speed of the current forming the magnetic field[47]. The induced voltage value is defined as in Eq.2.

$$v(t) = L\frac{di(t)}{dt} \quad (2)$$

In this relation, the value of L is the inductance of the corresponding coil. In addition, according to Faraday's law, the change in magnetic

flux φ and the number of turns N express the value of the induced voltage as given in Eq.3.

$$v(t) = N\frac{d\phi}{dt} \tag{3}$$

Using both equations, coil value L is calculated according to Eq.4.

$$L = \frac{N\phi}{I} \tag{4}$$

Here N is the number of turns, φ is the magnetic flux, and I is the current passing through the coil. The current equation of the coil is obtained according to Eq.5.

$$i(t) = \frac{1}{L}\int_{-\infty}^{t} v(x)dx \tag{5}$$

The inductance calculation of the coil is thus defined. But transformer, wireless energy transfer system, etc. The effects of the coils on each other change the inductance values of the coils. These effects are examined under the heading of mutual inductance.

2.2. Mutual Inductance Analysis

According to Ampere's law, it was stated that an electric current would create a magnetic field. According to Faraday's law, it was also stated that a voltage would be induced in a circuit surrounded by a time-varying magnetic field. This effect is much higher in circuits where the windings are opposite each other[47]. In the circuit shown in Figure 4, current i and magnetic flux are seen passing through a coil with N windings.

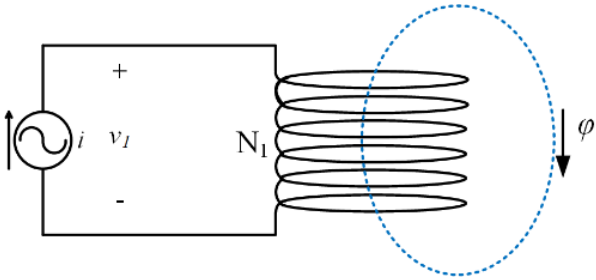

Figure 4. Magnetic flux surrounding the coil

The flux bond λ of the coil is expressed according to Eq.6 and Eq.7.

$$\lambda = N\phi \tag{6}$$

$$\lambda = Li \tag{7}$$

As can be seen here, the inductance value described in the previous section is constant. By arranging the equation, the magnetic flux can be rewritten in terms of current as given in Eq.8.

$$\phi = \frac{L}{N} i \tag{8}$$

According to Faraday's law, the voltage formed in the coil is proportional to the time change of the flux bond λ as given in Eq.9.

$$v = \frac{d\lambda}{dt} \tag{9}$$

The two coils come opposite, forming magnetically coupled circuits. The basic topology of the magnetically coupled circuit is shown in Figure 5.

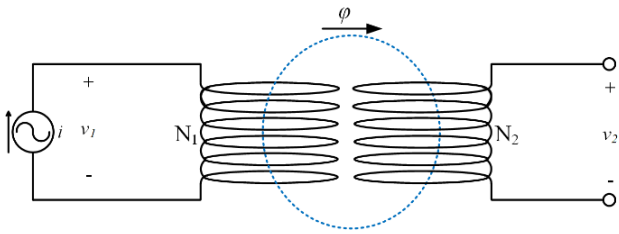

Figure 5. Magnetically coupled circuit

Current i_1 flows from the first coil with N_1 winding in the circuit. According to Faraday's law, when the magnetic flux created by the first coil is brought close enough to surround the second coil, voltage v_2 occurs in the second coil. The magnetic flux bond of the first coil is expressed according to Eq.10.

$$\lambda_1 = N_1\phi = L_1 i_1 \tag{10}$$

The voltage induced in the first coil is expressed as;

$$v_1 = \frac{d\lambda_1}{dt} = L_1 \frac{di_1}{dt} \tag{11}$$

Here L_1 is expressed as the self-inductance of the first coil. This is because, considering the effect of the second coil on the first coil, the inductance value of the first coil will change. When Eq.12 is rewritten for the second winding, the flux bond of the second winding is expressed as:

$$\lambda_2 = N_2\phi \tag{12}$$

According to Faraday's law, the voltage v_2 that will occur in the second winding is expressed according to Eq.13.

$$v_2 = \frac{d\lambda_2}{dt} = \frac{d}{dt}(N_2\phi) = \frac{d}{dt}\left(N_2(\frac{L_1}{N_1} i_1)\right) = \frac{N_2}{N_1} L_1 \frac{di_1}{dt} = L_{21} \frac{di_1}{dt} \tag{13}$$

As can be seen from the equation, the voltage v_2 is directly proportional to the rate of change of the current i_1 over time. This proportionality constant is expressed as mutual inductance L_{12}. If the flux bonds of the windings are rewritten as in Eq.14 and Eq.15;

$$\lambda_1 = L_1 i_1 + L_{12} i_2 \tag{14}$$

$$\lambda_2 = L_{21} i_1 + L_2 i_2 \tag{15}$$

According to Faraday's law, the winding voltages are obtained as seen in Eq.16 and Eq.17.

$$v_1 = \frac{d\lambda_1}{dt} = L_1 \frac{di_1}{dt} + L_{12} \frac{di_2}{dt} \tag{16}$$

$$v_2 = \frac{d\lambda_2}{dt} = L_{21} \frac{di_1}{dt} + L_2 \frac{di_2}{dt} \tag{17}$$

L_{12} and L_{21} values in the circuit represent mutual inductance values and are equal. The mutual inductance value is represented by the letter M.

$$L_{12} = L_{21} = M \tag{18}$$

The flux bond equations of the windings can be re-expressed with the self-inductance term due to the current of the winding itself and the term with mutual inductance due to the current of the other winding, as seen in Eq.19 and Eq.20.

$$\lambda_1 = L_1 i_1 - M i_2 \tag{19}$$

$$\lambda_2 = -M i_1 + L_2 i_2 \tag{20}$$

According to Faraday's law, the winding voltages are rearranged as given in Eq.21, and Eq.22 is obtained as;

$$v_1 = \frac{d\lambda_1}{dt} = L_1 \frac{di_1}{dt} - M \frac{di_2}{dt} \quad (21)$$

$$v_2 = \frac{d\lambda_2}{dt} = -M \frac{di_1}{dt} + L_2 \frac{di_2}{dt} \quad (22)$$

So far, the necessary expressions for the mutual inductance of any two coils have been explained. The analysis of mutual inductance of flat-layer circular coils is widely used in the literature for wireless charging of electric vehicles. The effect of two coils placed opposite each other was analyzed in the study by Maxwell [48]. Maxwell calculated the mutual inductance equation presented by Neumann using the elliptic integral. Neumann's inductance formula of two opposite conductors is given in Eq.23.

$$M = \frac{\mu_0}{4\pi} \int \int \frac{\overrightarrow{ds} \cdot \overrightarrow{ds'}}{r} \quad (23)$$

The equation d_s and d_s' contain the scalar product of the incremental sections of the conductors and the distance r between the outer diameters of the conductors. Maxwell calculated the mutual inductance value between two opposite conductor wires using the given equation in Eq.24.

$$M_{12} = \frac{\mu_0}{4\pi} \int \int \frac{cos\varepsilon}{r} \overrightarrow{ds} \cdot \overrightarrow{ds'} \quad (24)$$

The distance r between the outer diameters of the conductor wires in the equation is calculated using Eq.25.

$$r = \sqrt{{R_A}^2 + {R_B}^2 + c^2 - 2R_A R_B \cos(\varphi - \varphi')} \quad (25)$$

Here, R_A and R_B represent the radius value of each conductor wire, c represents the distance between the centers of the wires, and φ- φ' describes the angle parameters of the wires. The ε value in the equation expresses the difference of the angle parameters according to Eq.26.

$$\varepsilon = \varphi - \varphi' \tag{26}$$

According to the angle parameters of d_s and d_s' values, Eq.27 and Eq.28 is written as;

$$ds = R_B d\varphi \tag{27}$$

$$ds' = R_A d\varphi' \tag{28}$$

The given statements are brought together and take their final form in Eq.29.

$$M_{12} = \frac{\mu_0}{4\pi} \int_0^{2\pi} \int_0^{2\pi} \frac{R_A R_B \cos(\varphi-\varphi') d\varphi d\varphi'}{\sqrt{{R_A}^2+{R_B}^2+c^2-2R_A R_B \cos(\varphi-\varphi')}} \tag{29}$$

This obtained equation is calculated with the solution of the Elliptic Integral. There are two terms in the elliptical integral, K and E. Each term is calculated with a k_{12} coefficient, and its integral solution is provided. To solve this integral, it is expressed in the form in Eq.30[49].

$$M_{12} = \frac{2\mu_0\sqrt{R_A R_B}}{k_{12}} \left[\left(1 - \frac{k_{12}^2}{2}\right) K(k_{12}) - E(k_{12}) \right] \tag{30}$$

The k_{12} coefficient in the expression includes the parameters of the conductor wires and is calculated as in Eq.31.

$$k_{12}^2 = \frac{4R_A R_B}{(R_A R_B)^2 + c^2} \tag{31}$$

According to Eq.32 and Eq.33, the terms K and E of the elliptic integral are given as;

$$K = K\left(k_{12}, \frac{\pi}{2}\right) = K(k_{12}) = \int_0^{\frac{\pi}{2}} \frac{d\varphi}{\sqrt{1 - k_{12}^2 \sin^2 \varphi}} \tag{32}$$

$$E = E\left(k_{12}, \frac{\pi}{2}\right) = E(k_{12}) = \int_0^{\frac{\pi}{2}} \sqrt{1 - k_{12}^2 \sin^2 \varphi}\, d\varphi \tag{33}$$

Considering that the flat-layer circular coil consists of multi-turn conductor wires, the mutual inductance value of each turn of the conductor must be calculated. The coils are divided into (2N+1)x(2n+1) cells, and the sum of the mutual inductances obtained by calculating each cell separately is taken. The mutual inductance value obtained from these expressions is made for each turn, and the mutual inductance value between the coils is obtained using Eq.34[49].

$$M = \frac{N_1 N_2}{(2N+1)(2n+1)} \sum_{h=-N}^{h=N} \sum_{l=-n}^{l=n} M(h, l) \tag{34}$$

The arrangement of the coils whose mutual inductances will be calculated as a result of the equation is presented in Figure 6.

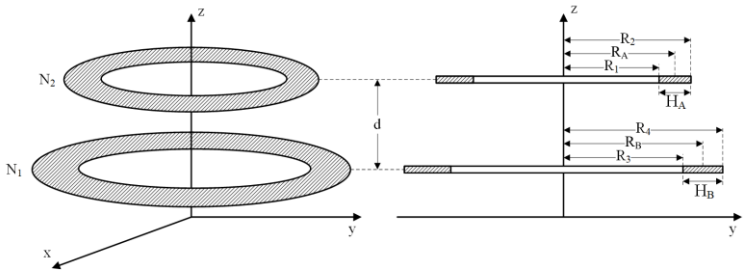

Figure 6. Representation of coil parameters for mutual inductance calculation of flat-layer circular coils

In the figure, R_1 and R_2 represent the inner and outer radii of the receiver coil. R_A is the distance of the average width of the receiver coil from the center of the coil, while H_A indicates the total width of the receiver coil. Likewise, R_3 and R_4 represent the inner and outer radii of the emitter coil. R_B indicates the distance of the average width of the transmit coil from the center of the coil, and H_B indicates the total width of the transmit coil. d represents the distance between the coils. There is an alignment difference between the coils, it is obtained by improving the previously given method. The distance difference between the center points between the coils according to the x-axis and y-axis and the distance change in the z-axis is calculated as expressed in Eq.35[50].

$$M(h,g,l) = \frac{\mu_0\sqrt{R_A(h)R_B(l)}}{\pi} x \int_0^{\pi} \frac{\left[\cos\theta - \frac{d}{R_B(l)}\cos\emptyset\right]\Psi(k_{12})}{\sqrt{V^3}} d\emptyset \qquad (35)$$

The variables used in the equation are given in Eq.36 -Es.41.

$$V = \sqrt{1 - \cos^2\emptyset \sin^2\theta - 2\frac{d}{R_B}\cos\emptyset\cos\theta + \frac{d^2}{R_B^2}} \qquad (36)$$

$$k_{12}{}^{2} = \frac{4\alpha V}{(1+\alpha V)^2+\xi^2} \quad (37($$

$$\xi = \beta - \alpha \cos \emptyset \sin \theta \quad (38)$$

$$\alpha = \frac{R_B(l)}{R_A(h)} \quad (39)$$

$$\beta = \frac{z(g)}{R_A(h)} \quad (40)$$

$$\Psi(k_{12}) = \left(\frac{2}{k_{12}} - k_{12}\right) K(k_{12}) - \frac{2}{k_{12}} E(k_{12}) \quad (41)$$

In the equations, R_A and R_B represent the average width of each coil, V represents the angular position obtained due to the alignment of the coils, Ψ the elliptical solution parameters, ∅ and θ the angular difference concerning the x-axis and y-axis. The distances of the average coil widths from the origin to the origin are found as given in Eq.42 and Eq.43.

$$R_A = \frac{R_1+R_2}{2} \quad (42)$$

$$R_B = \frac{R_3+R_4}{2} \quad (43)$$

In the equation, R_1 and R_2 show the receiver coil's inner radius and outer radius, and R_3 and R_4 show the transmitter coil's inner radius and outer radius. The mutual inductance (M) equation is used to calculate the total mutual inductance by using the additive expression of each (h,g,l) point. (h,g,l) points change the average radius values for each turn of the coils and are used to obtain the mutual inductance of each turn. Here is the variation of the mean radius for the transmitter coil is calculated as;

$$R_A(h) = R_A + \frac{H_A}{(2N+1)} h \quad (44)$$

In the expression, the value of h is taken as h=-N,…0,…N. The HA value in the equation indicates the difference between the outer radius (R_2) and the receiver coil's inner radius (R_1). Likewise, the mean radius change in the donor coil is calculated as;

$$R_B(l) = R_B + \frac{H_B}{(2n+1)} l \quad (45)$$

Again in this expression, the value of l is considered as l=-n,…0,…n. The HB value in the equation indicates the difference between the outer radius (R_4) and the transmitter coil's inner radius (R3). Calculating all these values, the effect on the z-axis resulting from the distance between the coils should be calculated. This value is expressed as;

$$z(g) = c + \frac{a}{(2K+1)} g \quad (46)$$

In the equation, the value of g is considered as g=-K,…0,…K. Here, a value indicates the conductor thickness of the coil. These given equations are used to obtain the total mutual inductance value as a result of the iteration for the number of cells (2N+1), (2K+1), and (2n+1).

2.3. Impedance Analysis

The WPT system is similar to an air-core transformer consisting of transmitting and receiving coils placed opposite each other. The system analysis, whose equivalent circuit is given in Figure 7, is carried out using the circuit analysis method.

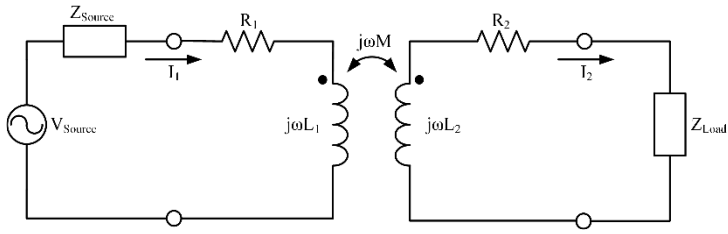

Figure 7. Air-core transformer equivalent circuit

In the circuit, the resistance of the transmitting coil R_1, the resistance of the receiver coil R_2, the self-inductance of the transmitting coil L_1, the self-inductance of the receiving coil L_2, the mutual inductance M between the two windings, the source voltage V_{Source}, the internal resistance of the source Z_{Source}, the load impedance Z_{Load}, the current through the transmit coil I_1 and the receiver The current through the coil is defined as I_2. If the environmental currents method in the equivalent circuit is applied as in Eq.47 and Eq.48;

$$V_{Source} = (Z_{Source} + R_1 + j\omega L_1)I_1 - j\omega M I_2 \quad (47)$$

is obtained. In equality is simplified as;

$$Z_{11} = Z_{Source} + R_1 + j\omega L_1 \quad (48)$$

$$Z_{22} = R_2 + Z_{Load} + j\omega L_2 \quad (49)$$

The flow equations are obtained as in Eq.50.

$$I_1 = \frac{Z_{22}}{Z_{11}Z_{22}+\omega^2M^2} V_{Source} \quad (50)$$

$$I_2 = \frac{j\omega M}{Z_{11}Z_{22}+\omega^2M^2} V_{Source} = \frac{j\omega M}{Z_{22}} I_1 \quad (51)$$

The impedance of the emitter circuit is obtained as in Eq.52 by subtracting the source impedance from the impedance of one cell.

$$Z_{in} = Z_{11}\frac{\omega^2M^2}{Z_{22}} - Z_{Source} \quad (52)$$

If the terms Z_{11} and Z_{22} are rewritten in the obtained equation;

$$Z_{in} = R_1 + j\omega L_1 + \frac{\omega^2M^2}{R_2+Z_{Load}+j\omega L_2} \quad (53)$$

is obtained. When attention is paid to equality, it is seen that the last term shows the effect of the receiver side. This term is in Eq.54;

$$Z_r = \frac{\omega^2M^2}{R_2+Z_{Load}+j\omega L_2} \quad (54)$$

Furthermore, is called the reflected impedance. As seen in the equation, the value that makes the reflected impedance zero is the mutual inductance value M, and it directly affects the circuit's input impedance.

3. EFFICIENCY IN MRCWPT SYSTEMS

The most important factors affecting the efficiency in the wireless charging system are the coupling coefficient k and the quality factor Q. The coupling coefficient is the ratio of the effect of the magnetic flux density between the transmit and receive coils on the other coil[43]. The relation between the coupling coefficient k and the mutual inductance value M between the coils is given in Eq.55.

$$k = \frac{M}{\sqrt{L_1 L_2}} \tag{55}$$

As seen in the equation, the mutual inductance M and the self-inductance L_1, L_2 values of the coils are essential for the coupling coefficient. Another factor affecting the efficiency of the system is the quality factor. The quality factor is directly proportional to frequency and inductance value and inversely proportional to the equivalent load resistance. As the equivalent resistance increases, the quality factor decreases. Depending on the coupling coefficient and the quality factor, the efficiency expression of the WPT system is given in Eq.56. As can be seen in the equation, the coupling coefficient affects exponentially, and the quality factor affects both the receive coil and the transmit coil separately.

$$\eta_{wpt} = \frac{k^2 Q_1 Q_2}{\left(1+\sqrt{1+k^2 Q_1 Q_2}\right)^2} \tag{56}$$

The efficiency expression can also be expressed depending on the circuit components. Since the current through the load I_L and the receiver circuit current I_2 are equal, the efficiency of the receiver circuit can be expressed as $\eta_{rec} = R_L/(R_L + R_2)$. The efficiency is given in Eq.57 [46] when the receiving circuit is operated at the resonant frequency[45].

$$\eta_{wpt} = \left(\frac{1}{1+\frac{(R_2+R_L)R_1}{\omega^2 M^2}} \frac{R_L}{R_L+R_2}\right) \tag{57}$$

The internal resistance of the receiver coil R_2, the load resistance R_L and the switching angular velocity ω do not change under constant

frequency. The only variable that affects the efficiency is the mutual inductance M. In this case, the resonance condition of the WPT system and the compensation of the mutual inductance M value, which disrupts the load compatibility of the E-class inverter, is necessary to increase the efficiency.

CONCLUSIONS

It has been emphasized that the most suitable method for wireless charging of electric vehicles is the Magnetic Resonance Coupling WPT system. The analysis of Mutual Inductance, which is the most critical parameter in the WPT system, is discussed in detail. The effect of different mutual inductance values to be obtained at different distances on the efficiency of the WPT system has been analyzed.

REFERENCES

1. Siqi L, Mi CC. Wireless Power Transfer for Electric Vehicle Applications. IEEE Journal of Emerging and Selected Topics in Power Electronics. 2015, 3, 4-17.
2. Azad A, Saha T, Zane R, Pantic Z. Design of Hybrid Energy Storage Systems for Wirelessly Charged Electric Vehicles. 2015 IEEE 82nd Vehicular Technology Conference (VTC Fall), Boston, USA, 2015. p. 1-5.
3. Mi C. Development of an Extermely Efficient Wireless EV Charge. 2015.
4. Weihan L, Han Z, Tianze K, Mi C. Inter-operability considerations of the double-sided LCC compensated wireless charger for electric vehicle and plug-in hybrid electric vehicle applications. 2015 IEEE PELS Workshop on Emerging Technologies: Wireless Power (WoW), Daejeon, South Korea, 2015. p. 1-6.
5. Deng J, Li W, Nguyen TD, Li S, Mi CC. Compact and Efficient Bipolar Coupler for Wireless Power Chargers: Design and Analysis. IEEE Transactions on Power Electronics. 2015, 30, 6130-40.
6. Barman SD, Reza AW, Kumar N, Karim ME, Munir AB. Wireless powering by magnetic resonant coupling: Recent trends in wireless power transfer system and its applications. Renewable and Sustainable Energy Reviews. 2015, 51, 1525-52.
7. Gati E, Kampitsis G, Manias S. Variable Frequency Controller for Inductive Power Transfer in Dynamic Conditions. IEEE Transactions on Power Electronics. 2017, 32, 1684-96.
8. Pellitteri F, Ala G, Caruso M, Ganci S, Miceli R. Physiological compatibility of wireless chargers for electric bicycles. 2015 International Conference on Renewable Energy Research and Applications (ICRERA), Palermo, .Italy, 2015. p. 1354-9.
9. Miller JM, Onar OC, Chinthavali M. Primary-Side Power Flow Control of Wireless Power Transfer for Electric Vehicle Charging. IEEE Journal of Emerging and Selected Topics in Power Electronics. 2015, 3, 147-62.

10. Hai J, Li W, Tabaddor M, Chris M. Optimization and safety evaluation of a 3.3 kW wireless EV charger. 2015 IEEE Transportation Electrification Conference and Expo (ITEC) Dearborn, Michigan, USA, 2015. p. 1-5.
11. Chen SH, Chang YC, Chen TY, Cheng YC, Wei HW, Hsu Ts, et al. Prolong Lifetime of Dynamic Sensor Network by an Intelligent Wireless Charging Vehicle. Vehicular Technology Conference (VTC Fall), 2015 IEEE 82nd, Boston, USA, 2015. p. 1-5.
12. Ni W, Collings IB, Wang X, Liu RP, Kajan A, Hedley M, et al. Radio Alignment for Inductive Charging of Electric Vehicles. IEEE Transactions on Industrial Informatics. 2015, 11, 427-40.
13. Kesler M. Highly resonant wireless power transfer: safe, efficient, and over distance. WiTricity Corporation. 2013, 1-32.
14. IEEE Standard Technical Specifications of a DC Quick Charger for Use with Electric Vehicles. IEEE Std 203011-20152016. p. 1-97.
15. Lim Y, Tang H, Lim S, Park J. An Adaptive Impedance-Matching Network Based on a Novel Capacitor Matrix for Wireless Power Transfer. IEEE Transactions on Power Electronics. 2014, 29, 4403-13.
16. Kim NY, Kim KY, Ryu YH, Choi J, Kim DZ, Yoon C, et al. Automated adaptive frequency tracking system for efficient mid-range wireless power transfer via magnetic resonanc coupling. Microwave Conference (EuMC), 2012 42nd European, Amsterdam, 2012. p. 221-4.
17. Zhu B, Li J, Hu W, Gao X. Review of Magnetic Coupling Resonance Wireless Energy Transmission. International Journal of u- and e-Service, Science and Technology. 2015, 8, 257-72.
18. Hui SYR, Zhong W, Lee CK. A Critical Review of Recent Progress in Mid-Range Wireless Power Transfer. IEEE Transactions on Power Electronics. 2014, 29, 4500-11.
19. Beh T, Kato M, Imura T, Hori Y. Wireless power transfer system via magnetic resonant coupling at fixed resonance frequency -power transfer system based on impedance matching-. World Electric Vehicle Journal. 2011, 4, 744-53.

20. Kim KY. Wireless power transfer: Principles and engineering explorations. InTech2012.
21. Vilathgamuwa DM, Sampath JPK. Wireless Power Transfer (WPT) for Electric Vehicles (EVs)—Present and Future Trends. Plug In Electric Vehicles in Smart Grids2015. p. 33-60.
22. SM.2303-1 RI-R. Wireless power transmission using technologies other than radio frequency beam. 2016.
23. Zhang W, White JC, Abraham AM, Mi CC. Loosely Coupled Transformer Structure and Interoperability Study for EV Wireless Charging Systems. IEEE Transactions on Power Electronics. 2015, 30, 6356-67.
24. Kurs A, Karalis A, Moffatt R, Joannopoulos JD, Fisher P, Soljačić M. Wireless Power Transfer via Strongly Coupled Magnetic Resonances. Science. 2007, 317, 83-6.
25. Karalis A, Joannopoulos JD, Soljačić M. Efficient wireless non-radiative mid-range energy transfer. Annals of Physics. 2008, 323, 34-48.
26. Wei X, Wang Z, Dai H. A Critical Review of Wireless Power Transfer via Strongly Coupled Magnetic Resonances. Energies. 2014, 7, 4316-41.
27. Liu C, Hu AP, Nair NKC. Modelling and analysis of a capacitively coupled contactless power transfer system. IET Power Electronics. 2011, 4, 808.
28. Lu F, Zhang H, Hofmann H, Mi C. A Double-Sided LCLC-Compensated Capacitive Power Transfer System for Electric Vehicle Charging. IEEE Transactions on Power Electronics. 2015, 30, 6011-4.
29. Dai J, Ludois DC. Capacitive Power Transfer Through a Conformal Bumper for Electric Vehicle Charging. IEEE Journal of Emerging and Selected Topics in Power Electronics. 2016, 4, 1015-25.
30. Yi KH. Electric field wireless power transfer with impedance transformation. 2016 IEEE International Conference on Consumer Electronics (ICCE), Berlin, 2016. p. 365-6.
31. Mi C. High power capacitive power transfer for electric vehicle charging applications. 2015 6th International Conference on Power Electronics Systems and Applications (PESA). IEEE, Hong Kong, 2015. p. 1-4.

32. Akuzawa Y, Tsuji K, Matsumori H, Ito Y, Ezoe T, Sakai K. A 95% efficient inverter with 300-W power output for 6.78-MHz magnetic resonant wireless power transfer system. 2015 IEEE MTT-S International Microwave Symposium, Phoenix, Arizona, USA, 2015. p. 1-3.
33. Luo Y, Yang Y, Chen Z. Self-tuning wireless power transmission scheme based on on-line scattering parameters measurement and two-side power matching. Sci Rep. 2014, 4, 4332.
34. Lin FY, Covic GA, Boys JT. Evaluation of Magnetic Pad Sizes and Topologies for Electric Vehicle Charging. IEEE Transactions on Power Electronics. 2015, 30, 6391-407.
35. Kisacikoglu MC, Kesler M, Tolbert LM. Single-Phase On-Board Bidirectional PEV Charger for V2G Reactive Power Operation. IEEE Transactions on Smart Grid. 2015, 6, 767-75.
36. Uddin MK, Ramasamy G, Mekhilef S, Ramar K, Lau YC. A review on high frequency resonant inverter technologies for wireless power transfer using magnetic resonance coupling. 2014 IEEE Conference on Energy Conversion (CENCON), , Johor Bahru, Malaysia, 2014. p. 412-7.
37. Waters B, Sample A, Smith J. Adaptive impedance matching for magnetically coupled resonators. PIERS Proceedings. 2012, 694-701.
38. Ibrahim M, Pichon L, Bernard L, Razek A, Houivet J, Cayol O. Advanced Modeling of a 2-kW Series-Series Resonating Inductive Charger for Real Electric Vehicle. IEEE Transactions on Vehicular Technology. 2015, 64, 421-30.
39. Ghate K, Dole L. A review on magnetic resonance based wireless power transfer system for electric vehicles. 2015 International Conference on Pervasive Computing (ICPC), Pune,India, 2015. p. 1-3.
40. Jiang W, Xu S, Li N, Lin Z, Williams BW. Wireless power charger for light electric vehicles. 2015 IEEE 11th International Conference on Power Electronics and Drive Systems, Sydney, Australia, 2015. p. 562-6.

41. Yang J-R, Kim J, Park Y-J. Class E Power Amplifiers using High-Q Inductors for Loosely Coupled Wireless Power Transfer System. Journal of Electrical Engineering and Technology. 2014, 9, 569-75.
42. Zhang X, Yuan Z, Yang Q, Li Y, Zhu J, Li Y. Coil Design and Efficiency Analysis for Dynamic Wireless Charging System for Electric Vehicles. IEEE Transactions on Magnetics. 2016, 52, 1-4.
43. Kim H, Song C, Kim D-H, Jung DH, Kim I-M, Kim Y-I, et al. Coil Design and Measurements of Automotive Magnetic Resonant Wireless Charging System for High-Efficiency and Low Magnetic Field Leakage. IEEE Transactions on Microwave Theory and Techniques. 2016, 1-18.
44. Sallán J, Villa JL, Llombart A, Sanz JF. Optimal design of ICPT systems applied to electric vehicle battery charge. IEEE Transactions on Industrial Electronics. 2009, 56, 2140-9.
45. Chopra S, Bauer P. Analysis and design considerations for a contactless power transfer system. 2011 IEEE 33rd International Telecommunications Energy Conference (INTELEC), Amsterdam, Netherlands, 2011. p. 1-6.
46. Shevchenko V, Husev O, Strzelecki R, Pakhaliuk B, Poliakov N, Strzelecka N. Compensation Topologies in IPT Systems: Standards, Requirements, Classification, Analysis, Comparison and Application. Ieee Access. 2019, 7, 120559-80.
47. Irwin JD, Nelms RM. Basic engineering circuit analysis. Wiley Publishing2008.
48. Maxwell JC. A Treatise on Electricity and Magnetism. Oxford Universtiy Press1881.
49. Babic S, Salon S, Akyel C. The mutual inductance of two thin coaxial disk coils in air. IEEE Transactions on Magnetics. 2004, 40, 822-5.
50. Babic SI, Akyel C. Calculating Mutual Inductance Between Circular Coils With Inclined Axes in Air. IEEE Transactions on Magnetics. 2008, 44, 1743-50.

CHAPTER 5

THE INCREASING IMPORTANCE OF ENERGY AND NUCLEAR ENERGY

Prof. Dr. Orhan ÇOBAN[1]

Lec. Ayşe ÇOBAN[2]

[1] Prof. Dr., Gaziantep University, Faculty of Economics and Administrative Sciences, Gaziantep, Turkey; ocoban@gantep.edu.tr; ORCID ID: 0000-0001-6137-8937.

[2]Gaziantep University, Oguzeli Vocational School of Social Sciences, Turkey; aysecoban@gantep.edu.tr; ORCID ID: 0000-0002-7844-7633.

.

INTRODUCTION

Energy is one of the most important indicators of economic growth and development. In order to meet their rapidly increasing energy needs, countries have started to turn to new energy sources that can be an alternative to primary energy sources. One of these alternative sources is nuclear energy. In this context, nuclear energy has been used in electricity production since the 1960s, and since the 1970s, nuclear energy has spread throughout the world. In the process until today, there have been intense discussions about the benefits and harms of nuclear energy. Those who highlight the harms of nuclear energy refer to nuclear accidents, while those who highlight the benefits state that nuclear energy is a necessity in meeting the energy needs of countries.

Turkey has entered a stable growth trend in recent years. Therefore, the energy demand is constantly increasing. Sustainable energy policies are needed in order to realize the economic, social and technological goals and to meet the increasing energy needs. Turkey can only supply 25% of its total energy needs from domestic sources. As it can be understood from here, Turkey is 75% foreign-dependent on energy. At the same time, energy policies are given great importance in Turkey, which is an energy corridor between east and west (Önce and Paksoy, 2015). Therefore, there is a serious trend towards alternative energy sources, especially renewable energy investments, in order to reduce the foreign dependency. In this context, nuclear energy has come to the fore as an alternative energy

source and nuclear power plant projects have started to be implemented. The first example of this is the Mersin/Akkuyu nuclear power plant.

The aim of this study is to reveal the current situation and to analyze the economic importance of the nuclear energy projects planned to be made in Turkey, taking into account the historical development of nuclear energy. In this context, first of all, the concept of nuclear energy will be explained. Then, the historical development of nuclear energy will be emphasized and its relations with the economy will be examined. Finally, nuclear energy in Turkey will be discussed and policies towards nuclear energy in Turkey will be discussed.

NUCLEAR ENERGY CONCEPT

Nuclear energy is a form of energy that occurs as a result of the splitting or merging of atomic nuclei. The fission reaction results in the splitting of atomic nuclei. The reaction that creates energy by the union of two large atomic nuclei is the fusion reaction. The use of energy produced by fission and fusion reactions is nuclear energy. It is also called core energy (Erdöşemeci, 2014: 21; Çetin, 2021: 5-7).

Electricity produced from nuclear power plants is safer than thermal and hydroelectric power plants. Although the establishment costs of nuclear power plants are higher than the others, their fuel and operating costs are lower (Ergün and Atay Polat, 2012: 37-38). The raw material of nuclear energy production is uranium and this element is used in nuclear power plants. Since it is an exhaustible element, alternative elements are sought to uranium. Thorium element is

considered as one of them. In this context, the operating mechanisms of nuclear power plants and thermal power plants are similar to each other. Nuclear power plants are classified under four headings as "Boiling Water", "Pressured Water", "Pressured Heavy Water" and "Gas Cooled" nuclear power plants (Acar and Boz, 2018: 3).

NUCLEAR ENERGY AND ECONOMY

The peaceful use of nuclear energy began in the 1930s. However, humanity first recognized nuclear energy in 1945 with the atomic bombs dropped on the Japanese cities of Hiroshima and Nagasaki by the USA. The first experimental nuclear reactor was built in 1942 by Enrico Fermi at the University of Chicago facility. In this context, the USA and the former Soviet Union have taken their places in history as the first countries to produce energy from nuclear energy. Although its historical development is not very old, there has been a rapid development in the use of nuclear energy. Today, nuclear energy is used in many fields, especially in industry, medicine and weapons industry (Temurçin and Aliağaoğlu, 2003: 26-27).

The top 10 countries in the distribution of nuclear power plants in the world by country are shown in Figure-1.

According to Figure-1, the USA is the country with the most nuclear power plants in the world with 93 reactors. The USA is followed by France with 56 reactors, China with 52 reactors, Russia with 38 reactors, Japan with 33 reactors, Republic of Korea with 24 reactors, India with 22 reactors and Canada with 19 reactors. As of December 2021, the total number of reactors in operation in the world is 442.

The construction of 54 nuclear reactors, 11 of them in China, 7 of them in India and 1 in Turkey, is continuing.

Figure 1: ***Top 10 Countries in Nuclear Power Plants in the World***

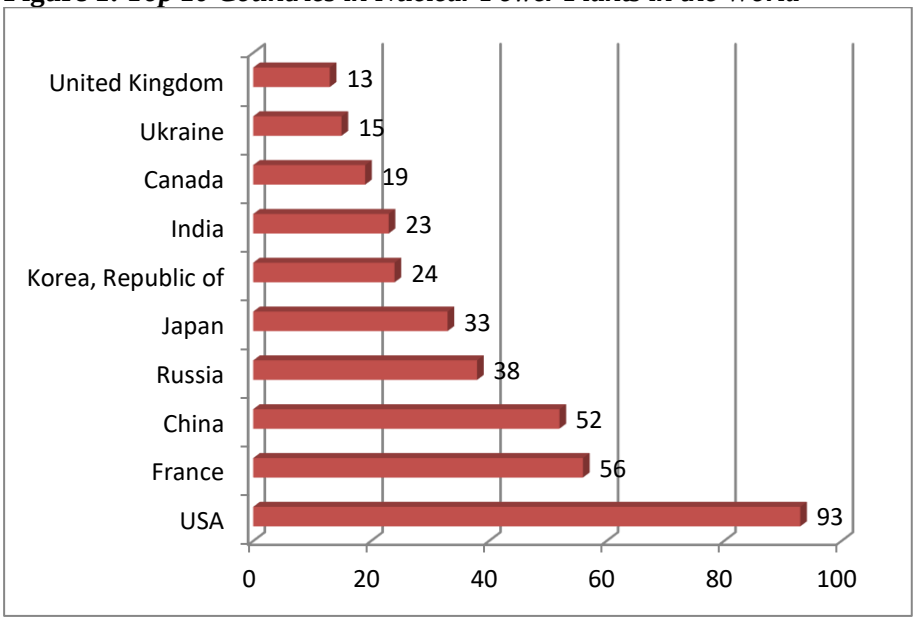

Source: IAEA, 2020.

Since the second half of the 20th century, many countries have sought to ensure energy security. The Oil Crisis in the 1970s accelerated these searches and nuclear energy became more and more important day by day. By the end of the 1980s, many nuclear power plants were established and started to operate. By the end of the 1980s, the demand for nuclear energy began to decline and this process continued in the 1990s. Three Mile Island in the USA in 1979 and Chernobyl nuclear energy accidents in Ukraine in 1986 are counted among the most important reasons for this stagnation (Kapluhan, 2015: 30-31). In this context, the Fukushima nuclear power plant

accident that occurred in Japan in 2011 is one of the important accidents in the historical development of nuclear energy (Koçak Güngör and Buldurur, 2017: 296).

Considering the distribution of currently active reactors by region, Western Europe ranks first with 26%. Western Europe is followed by North America and Far East countries with 25% (Nuclear Energy World, 2018). As it can be understood from here, the European Union countries have almost one third of the nuclear installed power. In this context, the country with the highest number of nuclear power plants is France, and it sees nuclear energy as the most important resource due to its insufficient own resources. The fact that the rate of nuclear power reactors is 0% in African countries is another indicator of the poverty experienced in these regions (Yıldırım and Örnek, 2007: 35).

The future of nuclear energy; energy demand, carbon emission targets, economic competition with fossil fuels, environmental sensitivities and public attitudes. In the coming years, important studies are carried out to improve the performance of other energy systems. In this context, new nuclear power plants that can compete with alternative energy sources are being designed. In addition, studies are carried out both to ensure security and to increase energy production (Eral, 2015: 13).

The thing that makes the decision makers think about nuclear energy investments the most is the high costs of establishment. When the installation and economic life of each nuclear power plant is completed, the dismantling costs are around 3 billion dollars. Despite

its cost, nuclear energy has become a preferred type of energy due to its contribution to the reduction of energy unit costs as well as reducing foreign dependency. In particular, the decrease in energy unit costs will positively affect the competitiveness of both micro and macro scales. In the final analysis, nuclear energy contributes to the increase of both individual and social welfare (Ergün and Atay Polat, 2012: 41).

NUCLEAR ENERGY IN TURKEY

Although the direct effect of growth on energy demand is low in developed countries, energy demand increases rapidly with growth in developing countries such as Turkey (Altunakar, 2014: 123). Recently, the thoughts that nuclear energy can be a solution to meet the increasing energy demand have started to increase (Üner et al., 2017: 34). In this framework, it is estimated that the energy demand will increase by 50-60% in the world and by 160% in Turkey in 2030 (IAAE, 2020). In line with this information, Turkey's dependence on foreign energy will increase in the coming periods. Nuclear energy is thought to be an important alternative in reducing foreign dependency on energy. It is also considered that Turkey will have a more advanced technology with nuclear technology (Ergün and Atay Polat, 2012: 51).

Turkey has been in search of nuclear energy for more than 50 years (Güneş, 2015: 651-652). Studies on this subject were first started in 1956, and a one MW research reactor was put into operation at the Büyükçekmece Nuclear Research and Training Center. Turkey became a member of the International Atomic Energy Agency (IAEA)

in 1957. In 1982, the Atomic Energy Commission was reorganized as the Atomic Energy Agency. The duties of the institution are to obtain electricity from nuclear energy and to give the necessary license to nuclear power plants (Karakuzu, 2011: 55-56).

In 1972, a nuclear power plant was planned to be built in Mersin/Akkuyu under the supervision of the Turkish Atomic Energy Agency, but the project could not be implemented for various reasons. The project, which was brought to the agenda again in 1993, was canceled again in 2000. It is thought that political and economic factors are effective in the cancellation of nuclear power plant projects (Yıldırım and Örnek, 2007: 35).

Agreements were signed with Russia to establish a nuclear power plant in Mersin Akkuyu in 2010, and with Japan in 2013 in Sinop (Koçak Güngör and Buldurur, 2017: 301-302). The agreement with Japan was canceled due to financing problems. With the agreement signed between Turkey and Russia in 2015, it was decided by ROSATOM to build a nuclear power plant in Mersin/Akkuyu. The construction of this power plant is still ongoing. The total cost of the power plant is approximately 20 billion dollars. It is planned to produce an average of 35 billion kilowatt-hours of electricity annually when it serves at full capacity. This figure means all of Istanbul's energy needs and 10% of Turkey's (Kaya and Göral, 2016: 425-434).

CONCLUSION

The aim of this study is to reveal the current situation and to analyze the economic importance of the nuclear energy projects planned to be made in Turkey, taking into account the historical development of nuclear energy. Although the use of nuclear energy for peaceful purposes started in the 1930s, humanity was first introduced to nuclear energy with the atomic bombs dropped on Hiroshima and Nagasaki in 1945. The USA and the former Soviet Union took their place in history as the first countries to produce energy from nuclear energy. The country with the most nuclear power plants in the world is the USA with 98 reactors. As of 2021, the total number of reactors in operation in the world is 442, and the construction of 54 nuclear reactors continues.

Turkey has been in search of nuclear energy since the 1950s. Finally, with the agreement signed between Turkey and Russia in 2015, the construction of a nuclear power plant in Mersin/Akkuyu started. It is estimated that the first reactor of the power plant will start energy production in 2023. It is predicted that the power plant, which has a total cost of approximately 20 billion dollars, can meet 10% of Turkey's energy needs if it serves at full capacity.

REFERENCES

Acar, Vedat and Mustafa Fatih Boz (2018). "IFRS ve FASB Açısından Nükleer Güç Santrali, Elektrik Üretim İşletmelerinde Uygulanan Özellikli Muhasebe Konuları". *Ömer Halisdemir Üniversitesi İktisadi ve İdari Bilimler Dergisi* 11(1): 83.

Altunakar, S. Şehnaz (2014). *Enerji Ekonomisinin Yapısal Sorunları ve Nükleer Enerji Örneği*. Doktora Tezi, Denizli: Pamukkale Üniversitesi Sosyal Bilimler Enstitüsü.

Çetin, Emrah (2021). *Elektrik Enerjisi Üretimi*, https://pbs.bozok.edu.tr /user_dosyalar/558-93611.pdf, (Available at: 15.02.2021).

Eral, Meral (2015). *Nükleer Güç Santralleri ve Ülkemiz*. http://www.kmo.org.tr/ resimler/ekler/1423037b0f99b51_ek.pdf, (Available at: 25.11.2018).

Erdöşemeci, Feyza (2014). *Nükleer Güç Santrallerinin Çevre Etiği Açısından İrdelenmesi*. Yüksek Lisans Tezi, Ankara: Gazi Üniversitesi Fen Bilimleri Enstitüsü.

Ergün, Suzan and Melike Atay Polat (2012). "Nükleer Enerji ve Türkiye'ye Yansımaları". *İnönü Üniversitesi Uluslararası Sosyal Bilimler Dergisi* 1(2): 37-52.

Güneş, İsmail (2015). "Nükleer Enerji Türkiye İçin Doğru Bir Tercih Mi?". *Uluslararası Avrasya Ekonomileri Konferansı*, 9-11 Eylül, Kazan, Rusya, https://www.avekon.org/papers/1426.pdf, (Available at: 10.01.2021).

IAEA (Internetional Atomic Energy Agency) (2020). *https://pris.iaea.org/PRIS/ WorldStatistics/OperationalReactorsByCountry.aspx*, (Available at: 10.11.2020).

Kapluhan, Erol (2015). "Nükleer Enerjide Yeni Yaklaşımlar: Toryum ve Enerji Kaynağı Olarak Kullanımı". *İnternational Journal Of Eurasia Social Sciences* 6(21): 29-47.

Karakuzu, Taner (2011). "Türkiye'nin Enerji Siyaseti: Nükleer Enerji Dışa Bağımlılığı Yenmede Bir Kilometre Taşı mı?". *Elektronik Siyaset Bilimi Araştırmaları Dergisi* 2(1): 48-77.

Kaya, Ferat and Emirhan Göral (2016). "Türkiye'nin Nükleer Enerji Politikası". *Akademik Bakış Dergisi* 57: 421-438.

Koçak Güngör, Merve and Mesture Aysan Buldurur (2017). "Türkiye'de Enerji Potansiyelinin Doğru Kullanımı: Nükleer Enerji Yatırım Projelerinin Değerlendirilmesi". *İdealkent* 8(21): 292-314.

Nuclear Energy World (Nükleer Enerji Dünyası) (2018). *İşletme Halindeki Reaktörlerin Bölgelere Göre Dağılımı*. http://www.nukleer.web.tr/guncel_veriler/bolgeler.html, (Available at: 15.03.2021).

Önce, Asım Günal and Sadettin Paksoy (2015). "Trans Anadolu Doğal Gaz Boru Hattı Projesi'nin (TANAP) Bölge Ekonomisi ve Barışı Açısından Önemi", *I. Uluslararası Kafkasya-Orta Asya Dış Ticaret ve Lojistik Kongresi Bildiriler Kitabı*, 733-750.

Temurçin, Kadir and Alpaslan Aliağaoğlu (2003). "Nükleer Enerji ve Tartışmalar Işığında Türkiye'de Nükleer Enerji Gerçeği". *Coğrafi Bilimler Dergisi* 1(2): 25-39.

Üner, Sinem, Adnan Kan and Hüseyin Akkuş (2017). "Nükleer Santrale Yönelik Tutum Ölçeğinin Geliştirilmesi: Geçerlik ve Güvenirlik Çalışması". *Eğitim ve Toplum Araştırmaları Dergisi* 4(1): 34.

Yıldırım, Metin and İbrahim Örnek (2007). "Enerjide Son Seçim: Nükleer Enerji". *Gaziantep Üniversitesi Sosyal Bilimler Dergisi,* 6(1): 32-44.

CHAPTER 6

AN INVESTIGATION THE EFFECTS OF THE HYDROPOWER PLANTS ON CLIMATE CHANGE AND ENVIRONMENTAL ISSUES IN TURKEY

Prof. Dr. Ibrahim YUKSEL[1]

[1]Istanbul Rumeli University, Faculty of Engineering and Natural Sciences, Department of Civil Engineering, Istanbul Turkey, E-mail: yukseli2000@yahoo.com.ORCID: https://orcid.org/0000-0002-9856-8133

While Starting

Many countries in the world have played an important role in protecting the environment by reducing their greenhouse gas emissions. However, these efforts need to increase gradually all over the world.

The rapid increase in energy production and consumption causes some environmental problems both locally, regionally and globally. For this reason, it is necessary to turn to renewable and sustainable clean energy sources in energy production.

Hydro energy is one of the renewable and sustainable clean energy sources. The hydroelectric energy potential in the world meets about one-fifth of the total electrical energy. This rate is around 25% in Turkey. But, Turkey imports more than half of its energy needs, air pollution is at the top of the environmental problems in the country.

On the other hand, Turkey has many advantages both in terms of natural energy resources and geographical location. For this reason, Turkey has an active role in the development of renewable and sustainable energy resources. In this study, the environmental effects of hydroelectric power plants in Turkey are investigated.

INTRODUCTION

If the technology in energy production in the world remains constant and the energy need and consumption increase rapidly, it will be difficult to prevent environmental problems.

However, in order to ensure energy efficiency in the world, energy production, transmission, distribution and consumption must have sustainable policies.

Because the need to control atmospheric emissions of greenhouse and other gases will increasingly need to be based on efficiency in energy generation, transmission, distribution and consumption in the country.

It is very well known that with the increasing population, the energy needs in the world are constantly increasing and the demand for electrical energy continues to increase rapidly. As a result of this; Much of the world's energy market has relied on fossil fuels, which are low-cost but non-renewable and unsustainable.

In order to eliminate this bad picture, it is necessary to turn to renewable and sustainable clean energy. Hydropower is one of the cleanest energies in the world. With its hydro energy rich water resources, Turkey has an important role of many countries in the world for renewable and sustainable energy production.

In a study, it is mentioned that the total exploitable hydro potential in the world is at least six times higher [1,2]. Therefore, it is necessary to evaluate this potential in the countries, to increase clean energy production and to prevent climate change by minimizing environmental problems. Because hydropower is the type of energy that has the least impact on environmental problems and climate change.

ENERGY UTILIZATION IN TURKEY

Some of the energy sources in Turkey are hard coal, lignite, asphalt, oil, natural gas, hydropower, geothermal, wood, animal & plant wastes, solar and wind energy. The proven reserves of lignite, the most abundant domestic energy source, is 7300 million tons and found in almost all of the country's regions. Lignite has the largest percentage in total energy production with its 42.5% share. After lignite, wood has the greatest share in total energy production with its 20% and oil accounts for 13%, 12.4% hydro and the final 15% includes animal wastes, solar, hard coal, natural gas, geothermal electricity and geothermal heat [1,3-7]. Figure 1 shows that the total energy production and consumption in Turkey.

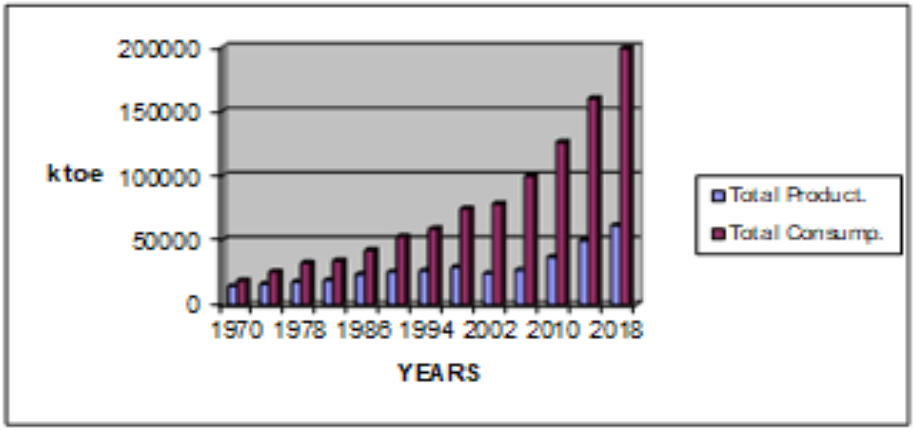

Figure 1. Total energy production and consumption in Turkey

In Turkey, MENR carries out general energy planning studies using the 'MAED' demand model, and TEIAŞ (Turkish Electricity Transmission Inc.) carries out energy production expansion planning studies using the DECADES model. Projections of medium and long-

term overall electricity demand are made using the MAED model. This model considers a detailed analysis of social, economic and technical systems. The model is based on three different scenarios: low, medium and high case.

Projecting the energy demand in the world correctly is very important because decisions involving large investments are based on these estimates [8-12].

Turkey Electricity Transmission Inc. (TEIAŞ), on the other hand, prepares long-term energy production plans by taking into account the demand results obtained with the DECADES model, which is used by the MAED model.

For example, TEIAS estimated that while the installed power in Turkey was 57,551 MW in 2010, this power will increase to 117,240 MW in 2020, and similarly, the installed hydroelectric capacity will increase from 18,943 MW in 2010 to 34,092 MW in 2020.

Since the last ten years, Turkey has been making great efforts to develop its full economic potential, especially in energy. In recent years, the most important developments in Turkey's energy production are seen in hydroelectric, geothermal and solar energy. The most important share among these belongs to hydropower.

However, on the other hand, the share of renewable and sustainable energy sources in total energy consumption (TFEC) has decreased due to the decrease in non-commercial use of biomass in the country and the increasing role of natural gas in the system [1,3-7,13].

Turkey has recently declared that it will reopen its nuclear program in order to respond to the increasing demand for electricity and to avoid the increasing dependence on energy imports.

However, Turkey does not currently have any nuclear power plants in operation or under construction, but has a long-standing nuclear research programme and has been considering nuclear power for many years.

Because as in many developed and developing countries in the world, nuclear energy maintains its importance in Turkey today.

The 2009 Electricity Market and Security of Supply Strategy envisages a contribution from nuclear power by 2020. A number of steps have been taken over recent years to prepare the legal and institutional framework needed for a nuclear programme.

A competitive tendering process for the construction of up to 5000 MWe of nuclear capacity was launched in early 2008. However, only one bid was received. Following legal challenges to the process, in November 2009 it was announced that the tender had been cancelled.

Direct negotiations have been continuing with potential suppliers, and in May 2010 an agreement was signed with the Russian Federation to build the country's first nuclear power plant [1,8,9].

Consumption of primary energy reached 119 641 ktoe as of the end of 2013 with an annual average increase of 2.9% while electricity consumption reached 219.3 billion kWh with an annual average increase of 4.6%.

However, in recent years, while energy consumption has increased at a high rate in Turkey, hydropower production has also increased. Because the main resources for hydroelectric generation in the country are quite abundant and rich and these resources represent about 20-30% of the total production. [1, 3-7].

RENEWABLE ENERGY IN TURKEY

In generally, firewood and animal waste which are the form of the biomass is mostly used as the main fuel for heating and cooking in urban and rural areas [14, 15]. The use of vegetable oils obtained from biomass as a fuel alternative has great economic, environmental and energy benefits for Turkey. In addition, since they constitute approximately 90% of diesel fuel, vegetable oils which also have heating value, can be seen as an alternative to biodiesel fuel.

In terms of geothermal energy, Turkey is one of the countries with significant potential. There is approximately 2000 MWe of geothermal energy in Turkey and the total geothermal heating capacity is approximately 31,500 MWth. Currently, the total geothermal heating capacity in the country is approximately 1220 MWth, which can meet the heating needs of 147,000 households. This value is expected to reach 7700 MWth in the early 2020s and meet the heating needs of approximately 1.2 million households [26-28].

However solar energy is the most important renewable energy source and the potential of solar energy is very high in Turkey, this sector has not been commercialized in the country [16].

While the heating energy required for household in Turkey, is approximately 60% of the total energy which is need in the country, on the other hand the energy demand for cooling in buildings increases rapidly in the southern region of the country during summer seasons. This is due to the general climatic and architectural boundary conditions, as well as increased internal cooling load and higher comfort requirements.

On the other hand, in terms of wind energy, Turkey has a good position in the world. Especially there are a few cities with very high wind speed and theoretical power of around 1000-3000 kWh/(m^2.year). Some of the regions with the most significant potential for wind energy in Turkey are the Marmara Sea region, the Mediterranean coast, the Aegean Sea coast and the Central Anatolia regions.

Although solar energy, as a renewable and sustainable energy type, has a high potential in the country, energy production in this area has not yet reached the desired level.

HYDROPOWER IN TURKEY

Since hydroelectric power plants are clean power generation plants, they contribute to reducing air pollution and slowing global warming. No other air pollutants or toxic wastes are produced. It also supports hydroelectricity, energy security and price stability.

Theoretically, Turkey's hydroelectric potential is 16% of Europe and 1% of the world. Hydropower is one of the ideal types of energy.

Because hydropower has low operating and maintenance costs, high efficiency and long project life [1,9-12,17].

The gross theoretical hydroelectric potential in Turkey is 433 billion kWh and approximately half of this potential (216 billion kWh) constitutes the technical potential [28]. The economically viable potential is approximately 140 billion kWh.

However, while the annual average energy consumption per capita in the world is 2,500 kWh, this amount in Turkey has exceeded the world average and reached approximately 2,900 kWh.

According to the statistical evaluations; The annual increase in energy consumption in Turkey is 8-10% excluding recession years [1,3,4,18]. Currently, Turkey produces around 48,000 GWh/year, which corresponds to approximately 35% of the economically viable hydroelectric potential. This energy is produced in 172 hydroelectric power plants with a total installed power of 13,700 MW [12].

On the other hand, at the moment about 150 hydroelectric power plants are under construction 8.600 MW of installed capacity to generate average annual 20.000 GWh representing 14% of the economically viable potential.

In addition, in order to evaluate the installed power of 22,700 MW in the future, studies for the establishment of 1418 more hydroelectric power plants have been started. As a result of these studies, the number of hydroelectric power plants will have increased to 1738 and their installed power will have increased to 45,000 MW. Thus, Turkey

will benefit from the economically viable hydroelectric energy potential at the maximum level (Table 1).

Table 1. Status of economically viable potential of hydroelectric power in Turkey

Status of Hydroelectric Power	Number of hydro power plants	Total installed capacity MW	Average Annual Generation (GWh/year)	Ratio (%)
In operation	172	13 700	48 000	35
Under construction	148	8 600	20 000	14
In program	1 418	22 700	72 000	51
Total potential	1 738	45 000	140 000	100

South-eastern Anatolia Project (GAP), which is one of the largest projects in the world and covers an agricultural land of 3.0 million hectares, not only produces a large amount of electrical energy, but also irrigates very large lands. More than half of the total irrigated land in Turkey is irrigated by the GAP which contains 22 dams and 19 hydroelectric power plants. GAP is located in the Euphrates and Tigris Basins and has a total electricity production capacity of 27 billion kWh and an irrigation capacity of 1.7 million hectares.

On the other hand, approximately 50% of the additional potential of 38 TWh in Turkey can be realized as small hydroelectric power (SHP) with installed capacities below 10 MW.

Currently, the share of small hydroelectric power plants in total hydroelectricity production is approximately 3%, but this rate will

reach 15% with the increase to be achieved in the 126 TWh/year usable energy potential with new projects [1,11,12,17,19].

RENEWABLE ENERGY AND CLIMATE CHANGE IN TURKEY

It is well known that the carbon emissions from any country contribute equally to the pressure on the global climate. Although Turkey has grown more rapidly among OECD countries, the main reason for the relatively rapid growth in emissions has been both the increase in energy use per capita and the very different evolution in the greenhouse gas intensity of the economy [20-24].

The Turkish government is now in the process of developing a strategy to reduce the growth of greenhouse gases. This strategy will be elaborated in the context of Turkey's adhesion to the United Nations Framework Convention on Climate Change (UNFCCC).

The importance of energy resources is increasing day by day in Turkey as well as in countries that increase in population and intensify industrialization. Renewable and sustainable energy types should be developed and expanded in order to reduce air pollution, reduce carbon emission volume and prevent climate change. One of the renewable and sustainable energy sources is hydropower.

Since total renewable energy supply declined from 1990 to 2004, due to a decrease in biomass supply the composition of renewable energy supply has changed.

As a result of this; some types of energy such as hydropower, wind power and solar energy are beginning to claim market share. Table 2 shows renewable energy supply and projections for future in Turkey [6,25,26].

Table 2. Renewable Energy Supply in Turkey

Renewable Energy Sources	2000	2005	2010	2015	2020
Primary energy supply					
Hydropower (ktoe)	2 656	4 067	4 903	7 060	9 419
Geothermal, solar and wind (ktoe)	978	1 683	2 896	4 242	6 397
Biomass and waste (ktoe)	6 457	5 325	4 416	4 001	3 925
Renewable energy production (ktoe)	10 091	11 074	12 215	15 303	19 741
Share of total domestic production (%)	38	48	33	29	30
Share of TPES (%)	12	12	10	9	9
Generation					
Hydropower (GWh)	30 879	47 287	57 009	82 095	109 524
Geothermal, solar and wind (GWh)	109	490	5 274	7 020	8 766
Renewable energy generation (GWh)	30 988	47 777	62 283	89 115	118 290
Share of total generation (%)	25	29	26	25	25
Total final consumption					
Geothermal, solar and wind (ktoe)	910	1 385	2 145	3 341	5 346
Biomass and waste (ktoe)	6 457	5 325	4 416	4 001	3 925
Renewable total consumption (ktoe)	7 367	6 710	6 561	7 342	9 271
Share of total final consumption (%)	12	10	7	6	6

CONCLUSIONS

In the last decade, Turkey has made a positive step towards implementing future energy efficiency policies by drafting the Energy Efficiency Strategy Paper, which includes indicative sectorial targets.

It is fundamental to complete the energy projects, in particular the hydroelectricity power plant projects, covered by the public investment program with the lowest costs and in the fastest manner.

Hydropower is a renewable form of energy since it uses the power of flowing water, without vested or depleting it in the generation of energy.

Since Turkey imports a significant part of its energy, the country can minimize this import by using other natural resources such as wind and sun, especially water resources.

For this, it should use the hydro energy potentials of both large and small rivers in 26 main basins in technical and economic terms at the maximum level.

In the use of hydro energy potential, it should concentrate on small hydro power plants called river type hydroelectric power plants on small rivers.

Because small hydro power plants produce energy without accumulating water, the environmental impact of these power plants is negligible, and besides creating employment for the unemployed people in that region; They make significant contributions to both the environment and the economy by enabling social activities such as

amateur fishing, picnic and recreation areas.

Therefore, hydroelectric power plants, which contribute to both the environment and the economy, will also prevent the occurrence of climate change or minimize its negative effects.

REFERENCES

[1] Yuksel, I., Kaygusuz, K. Renewable energy sources for clean and sustainable energy policies in Turkey. Renewable and Sustainable Energy Reviews 15 (2011) 4132– 4144.

[2] Abbasi, T., Abbasi, SA. Renewable energy sources: their impact on global warming and pollution. PHI Learning Private Limited, New Delhi, 2010.

[3] International Energy Agency (IEA). Energy Policies of IEA Countries: Turkey 2009 Review, OECD/IEA, Paris, 2010.

[4] MENR, Ministry of Energy and Natural Resources. Energy report of Turkey in 2008, Ankara, Turkey, http://www.enerji.gov.tr

[5] DPT, State Planning Organization. Ninth Development plan 2007-2013, Ankara, Turkey, 2006.

[6] Ministry of Environment and Forestry (MEF). First national Communication of Turkey on Climate Change (Eds. Apak, G and Ubay, B), pp. 60-150, Ankara, Turkey, 2007.

[7] TEIAS, Directorate-General of Turkish Electricity Transmission. 2009. Short history of electrical energy development in Turkey. http://www.teias.gov.tr

[8] IEA, International Energy Agency. World energy outlook 2009; IEA, Paris, 2009.

[9] Yuksel, I. Dams and Hydropower for Sustainable Development. Energy Sources, Part B 2009, 4: 100-110.

[10] Yuksel, I. Hydropower in Turkey for a clean and sustainable energy future. Renewable and Sustainable Energy Reviews 2008; 12: 1622-1640.

[11] Kaygusuz, K. Hydropower in Turkey: the sustainable energy future. Energy Sources, Part B 2009; 4: 34-47.

[12] DSI, State Hydraulic Works. Turkey water report, Ankara, Turkey, 2009.

[13] Yuksek, O.,Kömürcü, MI., Yuksel, I., Kaygusuz, K. The role of hydropower meeting the electric energy demand in Turkey. Energy Policy 2006; 34: 3093-3103.

[14] Balat, M. Use of biomass sources for energy in Turkey and a view to biomass potential. Biomass and Bioenergy 2005; 29: 32-41.

[15] Kaygusuz, K., Türker, MF. Biomass energy potential in Turkey. Renewable Energy 2002; 26: 661-678.

[16] EIE, Electrical Power Resources Survey and Development Administration. Potential of Turkish Wind and Solar Power, www.eie.gov.tr

[17] Yuksel, I. Development of hydropower: a case study in developing countries. Energy Sources, Part B 2007; 2: 113-121.

[18] Celiktas, MS., Gocar, G. A quadratic helix approach to evaluate the Turkish renewable energies. Energy 2009; 37: 4959-4965.

[19] Kaygusuz, K. Contribution of the Southeastern Anatolia Project (GAP) to irrigation and hydroelectric power production in Turkey. Energy Sources, Part B 2010; 5: 199-209.

[20] Greenhouse Gas Mitigation in Energy Sector for Turkey, Working Group Report, MENR Ankara, Turkey, 2005. www.iklim.cevreorman.gov.tr.

[21] Turkey Energy and Environmental Review, Task 7: Energy Sector Modeling, Prepared by G. Conzelman and V. Koritarov, Center for Energy, Environmental, and Economic
Systems Analysis (CEEESA), Argonne National Laboratory, August 2002.

[22] Kaygusuz, K. Energy and environmental issues relating to greenhouse gas emissions for sustainable development in Turkey. Renew Sustain Energy Reviews 2009; 13: 253-270.

[23] OECD, Organisation for Economic Co-Operation and development. OECD Economic Surveys: Turkey, OECD, Paris, 2008.

[24] OECD Organisation for Economic Co-Operation and development. Environmental Performance Reviews: Turkey, OECD, Paris, 2008.

[25] IEA, International Energy Agency, “Energy Policies of IEA Countries: Turkey 2005 Review”, 2005, OECD/IEA, Paris, France.

[26] MENR, Ministry of Energy and Natural Resources, “Energy Statistics in Turkey”, 2009, Available from http://www.enerji.gov.tr

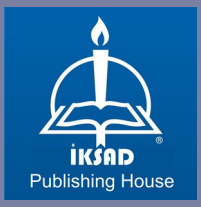

ISBN: 978-625-8061-10-9